NUMERICAL MODELLING OF FORCED CONVECTION IN A CAVITY DUE TO FINITE HEAT SOURCES

by

CHANDRA SEKHAR SRIGIRIRAJU

A thesis submitted to the

Graduate School-New Brunswick

Rutgers, The State University of New Jersey

In partial fulfillment of the requirements

For the degree of

Master of Science

Graduate Program in Mechanical and Aerospace Engineering

Written under the guidance of

Professor Yogesh Jaluria

And approved by

_____

_____

_____

New Brunswick, New Jersey

January 2015

ABSTRACT OF THE THESIS

NUMERICAL MODELLING OF FORCED CONVECTION IN A CAVITY DUE TO FINITE HEAT SOURCES

by

CHANDRA SEKHAR SRIGIRIRAJU

Thesis Director:

Professor Yogesh Jaluria

The problem of forced convection in a cavity is very well know and widely studied problem in the field of fluid mechanics. Numerous numerical techniques are present in literature which successfully simulate the fluid flow in a cavity upto a certain degree of accuracy. This present study is inspired by the physical phenomenon of fire in a ventilated aircraft cabin. Fluid flow inside a cavity is simulated numerically and the boussinesq approximation is considered in all the simulations. The governing equations and boundary conditions are solved using a commercially available code, namely Ansys Fluent. Benchmarking is done by solving the classic problem of a differentially heated two dimensional enclosed cavity. In first part of this study a rectangular cavity with vents is considered. Heat flux is applied to the bottom wall of the cavity. The inlet velocity and the heat flux applied are considered as parameters in the simulation. Different configurations of the cavity are considered by changing the location of the inlet and outlet vents. The simulations run are laminar as well as steady state in nature. The effects of buoyancy for varying heat fluxes are considered in detail. Comparative studies are done to find the best configuration in terms of heat removal. The second part of this study involves the numerical simulation of forced convection in a two dimensional aircraft fuselage cross-section with contains two seats. The seats are modelled as zero thickness walls and a temperature gradient is created by

applying heat flux to them. The simulations are transient as well as turbulent in nature. Different configurations of the cross-section are considered. The velocity vector fields and the temperature contours are studied in detail. Comparative studies are done to find the most efficient configuration for heat removal.

Acknowledgements

I would like to firstly thank my advisor Dr. Yogesh Jaluria for all his support and encouragement towards my thesis. He is a great mentor and always encouraged me to push my limits a little more. I thank him for giving me the wonderful opportunity to work on this project.

Sincere thanks to Dr. Mona Zebarjadi for being a great mentor and for the support and guidance during the summer. It was a privilege collaborating with her group and a great learning opportunity. Thanks to Dr. James Guo for being a part of the committee and reviewing my thesis. Special thanks to my lab mates Sunny Wong and Vijay Vembuli who have helped me during my research through their valuable suggestions and guidance.

I would also like to thank my dad S.N.V. Ramana Rao, my mom S. Radha Rao and my brother Swarup for their constant support and guidance throughout my academic career and without whom this work would have not been possible.

Table of Contents

LIST OF FIGURES

1. INRODUCTION

Fire in the air is considered as one of the most dangerous situations that a flight crew can be faced with in an aircraft. Without aggressive and immediate intervention by the flight crew, a fire on board an aircraft can lead to the catastrophic loss of that aircraft with in a very short period of time. Once a fire is self-sustained it is unlikely that the crew can extinguish it. The most common types of inflight fire are as follows [15]

Engine Fire

An engine fire is normally detected and contained satisfactorily by the aircraft fire detection and suppression systems. However, in certain cases, e.g. an explosive breakup of the turbine, the nature of the fire is such that onboard systems may not be able to contain or extinguish it. It may spread to the wings and fuselage.

Cabin Fire

A fire inside the cabin can usually be classified as a cabin fire. This type of fire is usually detected by the cabin crew or passengers and can be controlled or extinguished at an early stage. It is advisable to land the aircraft as fast as possible and carry out a detailed examination of the cause of the fire and the extent of the damage.

Hidden Fire

A hidden fire can be detected by the onboard fire detection systems or by the crew/passengers in the form of smoke or a hot spot inside the fuselage. This type is the most dangerous type among the three as they are difficult to locate and access in order to control them. If not controlled as soon as possible they can do extensive damage to the aircraft and can lead to loss of life and property.

A survey of commercial jet aircraft accident data shows that in-flight fire was responsible for the fourth highest number of on-board fatalities and was the seventh most frequent cause of accidents in 2005. According to the FAA, in the case of an in-flight fire

"…delaying the aircraft's decent by only two minutes is likely to make the difference between a successful landing and evacuation, and a complete loss of the aircraft and its occupants." [16] Hence it is of paramount importance to study the nature of propagation the flow involved during an in-flight fire. In broad terms it is done in the following ways:

1. Numerical simulation of the Navier Stokes equations along with the energy equations. Since most fires are turbulent in nature this is a computationally expensive process. Recent developments in the field of computational fluid dynamics like better models and advances in parallel computing have made this method much easier and highly reliable.
2. Scaled and full scale experiments performed in a controlled manner generally in labs or in the outside environment. These experiments are usually transient in nature. The help to get accurate data regarding the temperature and velocity profiles but is very expensive and time consuming to perform.
3. Zone models have been used for quite some time to simulate a fire in an enclosure. A zone model is a computer model that divides the domains/s in question into different control volumes or zones. The most common zone models is split a domain into two zones, an upper hot zone and a lower cold zone. The smoke stratifies into two distinct layers. Layers are assumed to be uniform throughout.

1.1 LITERARY REVIEW

The problem of heat transfer in a cavity is a well-known one and often has benchmark solutions. It has been studied extensively by many fluid dynamists. Mamun Molla (et all) [1] numerically simulate a 2D unsteady natural convection laminar flow in a square cavity. Their square cavity consists of insulated top and bottom walls, uniformly heated left wall and a uniformly cooled right wall. An upwind finite difference method and SOR iteration technique was used to discretize the 2D incompressible NS equations. The effect of buoyancy was also take into account. Effect of heat generation and varying Rayleigh numbers on streamlines and

isotherms was studied. Patterson (et all) [2] considered a closed rectangular 2d cavity. The upper and lower boundaries were insulated. A temperature gradient was applied between the left and right walls. The authors also incorporated the boussinesq approximation. Cavities of aspect ratios less than 1 were considered. A detailed analysis of the velocity and temperature fields was done with changing Rayleigh and Reynolds numbers. They concluded that for fixed aspect ratio and Pradtl number and increasing Ra number the flow changes from conduction dominated to convection dominated.

Nilesh (et al) [3] conducted a comparative study of the fluid flow with boussineq approximation and temperature dependent properties. A two dimensional enclosed rectangular cavity was considered with two opposite walls having a temperature gradient. They varied the Rayleigh number from 10^3 to 10^6. They found that the average Nusselt number is 10 to 15 % higher for the Temperature dependent case. The peak value of x velocity and y velocity are lower by 4 to 18 %. However the temperature profiles were not much different. In terms of computational resources they required 30 % higher for the temperature dependent simulations for steady state and 120 to 150% for transient simulations. Ivey (et all) [4] conducted an experiment to study the fluid flow in an enclosed cavity. In their setup the two vertical walls were kept at constant temperature (above the rest of the setup). The experiment was transient in nature. An oscillatory approach to the steady state temperature distribution was noticed. The temperature values fluctuated with high frequency near the walls of the cavity, where the boundary layers discharged into the cavity.

Ajay (et all) [5] studied the internal flow in a cavity by providing velocity at the top wall and a temperature gradient between opposite walls. Flow visualization was done using Thermochromic Liquid Crystals (TLC). They conducted the experiments by varying the Grashoff number between 10^7 to 10^9. The variation was achieved by changing the depth of the cavity and the temperature gradient applied. They concluded that heat transfer within the cavity is

independent of Gr/Re^2 in the range of 0.1 to 1000. Torrance (et all) [6] conducted a numerical simulation of fluid flow in a lid driven cavity. The effects of buoyancy were also considered. In their simulations Pr number and Reynolds number were kept fixed to 1 and 100 respectively. The simulation was performed for varying cavity aspect ratios and Grashoff numbers. Numerical accuracy and convergence of the numerical scheme was also reported. An interesting investigation was done by Khanafer (et all) [7] with regard to the effect of surrounding in open-ended enclosures. The authors performed 2D and 3D simulations of open ended structures for various Nusselt numbers.

Vahl Davis (et all) [8] perform a numerical simulation of natural convection between concentric vertical cylinders. The results were obtained for various Rayleigh numbers of up to 10^5 and Pradlt numbers in the range of 0.5 to 5. The aspect ratio and the radius ratio were also varied from 1 to 20 and 1 to 4 respectively. They noticed a flow reversal at Rayleigh numbers of 10^4 and 10^5. The velocity and temperature profiles were also studied. Bointoux (et all) [9] consider the case a fluid flow in a inclined cylinder which was differentially heated. The effects of inclination angle of the cylinder on the fluid flow were studied. 2D numerical simulations were carried for varying Rayleigh numbers. For inclination angle of 90 degrees (wrt to the vertical) the numerical results were compared with the analytical results. They were found to be in agreement till about Ra numbers of 6000. After that the numerical results deviate from the analytical results. The results were fairly in good agreement as they differed by less than 10 % on the maximum values at inclination angles between 120 degrees and 150 degrees. A detailed analysis of the flow at various inclination angles and Ra numbers was conducted. Mallinson (et all) [10] obtained a solution of the steady state Navier Stokes equations in 3D by numerical methods for natural convection in a rectangular cavity as a result of differential side heating. This problem had previously been treated as though it was 2D. The Boussinesq approximation has been applied to a viscous incompressible fluid. The simulations were carried out for varying Aspect ratios and

Rayleigh numbers. Teodosiu (et all) [11] performed a numerical simulation of flow in a cavity with an internal heat source. In their setup they had considered conduction, convection and radiation from the walls of the cavity. The realizable k epsilon model was used to model the turbulence inside the cavity. Their numerical model agreed with the experimental data.

Constantine (et all) [12] performed a full scale fire tests to simulate an aircraft post-crash environment. The toxicity levels produced by burning of seats and other material inside the aircraft were also studied. The time taken for flashover was also studied. Their setup consists of an aircraft fuselage which is divided into three portions, the interior which includes the cockpit and avionics, furnished section which includes the seats and the unfurnished section which is mostly empty space and is near the aft of the aircraft. In their setup the seat closet to the fuel source was first ignited, which is generally the case in aircraft fires. After some time the observed fire below the smoke layer remains localized and a two zone model persists until flashover. The toxicity levels before and after flashover is studied in detail. They found that the most important toxic gas produced by a cabin fire is CO. An interesting result is that incapacitation caused by exposure to toxic gases which are produced by flashover was shown to become more dominant as the distance from the fire origin increases and the closer one is to the floor.

Patel (et all) [13] perform a CFD analysis of the inflight fire that brought down the Swissair Flight 111 into the Atlantic Ocean. According to the crash investigation report, electrical arcing in the ceiling void cabling was most likely the cause of the fire. The authors used the SMARTFIRE CFD software to predict the possible behavior of airflow as well as the spread of fire and smoke within the aircraft. The code used 3d unstructured meshes to model irregular geometries. The solution was obtained using the SIMPLE algorithm. The results were obtained for two types of events namely pre fire and post-crash. All the simulations performed were transient in nature. This would be the first time when a fire model was used in an air crash investigation. This shows that CFD based fire analyses as a cost effective approach to

investigating complex flow scenarios and can be coupled with experimental data to get very accurate results.

2. MATHEMATICAL MODEL

Navier Stokes Equations in 3D in Cartesian coordinates is [14]

$$\rho\left(\frac{du_i}{dt} + u_j * \frac{\partial u_i}{dx_j}\right) = -\frac{\partial p}{\partial x_i} + \mu\left(\frac{\partial^2 u_i}{\partial {x_i}^2}\right) + \rho g_i$$

Continuity Equation is given as

$$\frac{\partial \rho}{\partial t} + \frac{\partial(\rho u_i)}{\partial x_i} = 0$$

Where

u_i Represents the velocity vector component in the i^{th} direction

ρ Represents the density of the fluid

p Represents the pressure

g_i Represents the gravity in the i^{th} direction

2.1 BOUSSINESQ APPROXIMATIONS

The Boussinesq approximation can be applied to a flow problem if the velocity of the flow is small, if not shock waves in the flow are considered, the vertical scale of the flow is not too large and the temperature differences in the fluid are small. In this approximation density changes due to temperature difference alone are considered.

2.2 REYNOLDS AVERAGED NAVIER STOKES EQUATIONS

The continuity equation takes the form as [14]

$$\frac{\partial(\overline{\rho})}{\partial x_i} = 0$$

The momentum equation takes the form as

$$\frac{D\overline{u_i}}{Dt} = \frac{-1}{\rho_0} * (\nabla\overline{p}) + \frac{\overline{\rho}}{\rho_0} * g_i + \vartheta * \nabla^2\overline{u_i}$$

Where

ρ_0 Represents a constant

The energy equation takes the form

$$\frac{D\overline{T}}{Dt} = k\nabla^2\overline{T}$$

Reynolds Averaged Equations of Motion (RANS)

$$\overline{u_i} = U_i + u_i$$

$$\overline{p} = P + p$$

$$\overline{\rho} = \rho + \rho'$$

$$\overline{T} = T + T'$$

Where

U_i , P , , T represent the mean velocity, pressure, density and temperature respectively

u_i , , ρ' , T' represent the fluctuations of velocity, pressure, density and temperature respectively.

$\overline{u_i}$, $\overline{p}$, $\overline{\rho}$, $\overline{T}$ represent the sum of mean quantities and their respective fluctuations

Consider the boussinesq approximation of the Navier Stokes equation

$$\frac{\partial \overline{u_i}}{\partial t} + \frac{\partial(\overline{u_j} * \overline{u_j})}{\partial x_j} = \left(\frac{-1}{\rho_0}\right) * \left(\frac{\partial \overline{\rho}}{\partial x_i}\right) - g * \left(1 - \alpha(\overline{T} - T_0)\right) * \delta_{i3} + \gamma * (\frac{\partial^2 \overline{u_i}}{\partial {x^2}_j})$$

$$\frac{\partial \overline{u}_i}{\partial x_i} = 0$$

$$\frac{\partial \overline{T}}{\partial t} + \overline{u_j} * \left(\frac{\partial \overline{T}}{\partial x_j}\right) = \frac{\partial \overline{T}}{\partial t} + \frac{\partial(\overline{u_j} * \overline{T})}{\partial x_j} = k * \left(\frac{\partial^2(\overline{T})}{\partial {x_j}^2}\right)$$

Consider the continuity equation

Substituting the above and taking the average we get

$$\frac{\overline{\partial \overline{u_i}}}{\partial x_i} = \frac{\partial(\overline{U_i + u_i})}{\partial x_i}$$

Which gives

$$\frac{\partial u_i}{\partial x_i} = \frac{\partial U_i}{\partial x_i} = 0$$

Consider the Momentum equation

Substituting the above and taking the average we get

$$\frac{\partial\overline{(\,U_i\,+\,u_i)}}{\partial t}+\frac{\partial\overline{(U_i+\,u_i)*(U_j+\,u_j)}}{\partial x_j}$$

$$=\frac{-1}{\rho_0}*\frac{\overline{\partial(P+p)}}{\partial x_i}-g*\overline{\Big(1-\,\alpha\big(\overline{T}+\,T'-\,T_0\big)\Big)*\delta_{i3}}+\,\vartheta*\frac{\overline{\partial^2(\,U_i+\,u_i)}}{\partial x_j^2}$$

Consider each term of the above term we get

$$\frac{\partial\overline{(\,U_i\,+\,u_i)}}{\partial t}=\frac{\partial U_i}{\partial t}$$

$$\frac{\partial\overline{(U_i+\,u_i)*(U_j+\,u_j)}}{\partial x_j}=\frac{\partial(\,(U_i*U_j)+\,\overline{u_i*u_j})}{\partial x_j}$$

$$\frac{-1}{\rho_0}*\frac{\overline{\partial(P+p)}}{\partial x_i}=\frac{-1}{\rho_0}*\frac{\partial P}{\partial x_i}$$

$$g*\overline{\Big(1-\,\alpha\big(\overline{T}+\,T'-\,T_0\big)\Big)*\delta_{i3}}=g*\Big(\,1-\,\alpha\big(\overline{T}-\,T_0\big)\Big)*\delta_{i3}$$

$$\vartheta*\frac{\overline{\partial^2(\,U_i+\,u_i)}}{\partial x_j^2}=\,\vartheta*(\frac{\partial^2U_i}{\partial x_j^2})$$

Upon adding we get

$$\frac{\partial U_i}{\partial t}+\,\frac{\partial(\,(U_i*U_j)+\,\overline{u_i*u_j})}{\partial x_j}=\frac{-1}{\rho_0}*\frac{\partial P}{\partial x_i}-\,g*\Big(\,1-\,\alpha\big(\overline{T}-\,T_0\big)\Big)*\delta_{i3}+\,\,\vartheta*(\frac{\partial^2U_i}{\partial x_j^2})$$

This can be written as

$$\frac{\partial U_i}{\partial t}+\,U_j*\frac{\partial(\,(U_i)}{\partial x_j}=\,-g*\Big(\,1-\,\alpha\big(\overline{T}-\,T_0\big)\Big)*\delta_{i3}+\frac{1}{\rho_0}*\left(\frac{\partial\overline{\tau_{ij}}}{\partial x_j}\right)$$

Or

$$\frac{\partial U_i}{\partial t}+\,U_j*\frac{\partial(\,(U_i)}{\partial x_j}=\,-g*\Big(\,1-\,\alpha\big(\overline{T}-\,T_0\big)\Big)*\delta_{i3}+\frac{1}{\rho_0}*\left(\frac{\partial(-P\delta_{ij}+2\mu\overline{S_{ij}}-\,\rho_0\overline{u_i*u_j})}{\partial x_j}\right)$$

Where

$$S_{ij} = \frac{1}{2} * \left(\frac{\partial U_i}{\partial x_j} + \frac{\partial U_j}{\partial x_i}\right)$$

Consider the energy equation

Substituting the above and taking average we get

$$\frac{\partial(\overline{T + T'})}{\partial t} + \frac{\partial\left(\overline{(U_j + u_j) * (T + T')}\right)}{\partial x_j} = k * \left(\frac{\partial^2\left(\overline{T + T'}\right)}{\partial {x_j}^2}\right)$$

Consider each term of the above equation we get

$$\frac{\partial(\overline{T + T'})}{\partial t} = \frac{\partial T}{\partial t}$$

$$\frac{\partial\left(\overline{(U_j + u_j) * (T + T')}\right)}{\partial x_j} = U_j * \left(\frac{\partial \overline{T}}{\partial x_j}\right) + \frac{\partial(\overline{u_j * T'})}{\partial x_j}$$

$$k * \left(\frac{\partial^2\left(\overline{T + T'}\right)}{\partial {x_j}^2}\right) = k * \left(\frac{\partial^2 T}{\partial x_j^2}\right)$$

Equation for the mean flow's Kinetic Energy per unit mass where

$$\overline{E} = \frac{1}{2} * U_i^2$$

Energy budget equation for $\overline{E}$ is

$$\frac{\partial \overline{E}}{\partial t} + U_j * \frac{\partial \overline{E}}{\partial x_j} = \frac{\partial\left(-U_j * P/\rho_0 + 2\vartheta U_i \overline{\delta}_{ij} - \overline{u_i u_j} U_i\right)}{\partial x_j} - 2\vartheta \overline{S}_{ij} \overline{S}_{ij} + \overline{u_i u_j} \frac{\partial U_i}{\partial x_j} - \frac{g}{\rho_0} \overline{\rho} U_3'$$

Where

$\frac{\partial \overline{E}}{\partial t} + U_j * \frac{\partial \overline{E}}{\partial x_j}$ Represents the Time rate of change of $\overline{E}$ following the mean flow

$\frac{\partial \left({}^{-U_j * P}/_{\rho_0} + 2\vartheta U_i \overline{\delta}_{ij} - \overline{u_i u_j} U_i \right)}{\partial x_j}$ Represents the transport of mean kinetic energy by pressure, viscous stresses and Reynolds stresses

$-2\vartheta \overline{S}_{ij} \overline{S}_{ij}$ Represents the direct viscous dissipation of mean kinetic energy via its conversion into heat

$\overline{u_i u_j} \frac{\partial U_i}{\partial x_j}$ Represents the shear production term

$-\frac{g}{\rho_0} \overline{\rho} U_3'$ Represents the loss to potential energy

Energy budget equation for $\overline{e}$ is

$$\frac{\partial \overline{e}}{\partial t} + U_j * \frac{\partial \overline{e}}{\partial x_j} = \frac{\partial \left(\overline{{}^{-u_j * p}/_{\rho_0}} + 2\vartheta \overline{u_i \delta_{ij}} - \frac{1}{2} \overline{u_i^2 u_j} \right)}{\partial x_j} - 2\vartheta \overline{S'}_{ij} \overline{S'}_{ij} - \overline{u_i u_j} \frac{\partial U_i}{\partial x_j} + g\alpha \overline{u_j T'}$$

Where

$\frac{\partial \overline{e}}{\partial t} + U_j * \frac{\partial \overline{e}}{\partial x_j}$ Represents the time rate of change of $\overline{e}$ following the mean flow

$\frac{\partial\left(\overline{-u_j * p}/\rho_0 + 2\vartheta\overline{u_i\delta_{ij}} - \frac{1}{2}\overline{u_i^2 u_j}\right)}{\partial x_j}$ Represents the spatial transport of turbulent kinetic energy via turbulent pressure fluctuations, viscous diffusion and turbulent stresses

$-2\vartheta\overline{S'}_{ij}\overline{S'}_{ij}$ Represents the viscous dissipation of turbulent kinetic energy

$-\overline{u_i u_j}\frac{\partial U_i}{\partial x_j}$ Represents the shear production term

$g\alpha\overline{u_j T'}$ Represents the buoyant production

2.3 k - ε MODEL

To solve the closure problem presents by the Reynolds Averaged Navier Stokes (RANS) equations various models are used to model the nature of turbulence. The k epsilon model is one of the most common turbulence models used. It involves the addition of two extra transport equations model the nature of turbulent flow.

First equation is as follows

$$\frac{\partial\overline{e}}{\partial t} + U_j * \frac{\partial\overline{e}}{\partial x_j} = \frac{\partial\left(\frac{\vartheta_T}{\sigma_e} * \frac{\partial\overline{e}}{\partial x_j}\right)}{\partial x_j} - \overline{\varepsilon} - \overline{u_i u_j}\frac{\partial U_i}{\partial x_j}$$

Second equation is as follows

$$\frac{\partial\overline{\varepsilon}}{\partial t} + U_j\frac{\partial\overline{\varepsilon}}{\partial x_j} = \frac{\partial(\frac{\vartheta_T}{\sigma_\varepsilon} * \frac{\partial\overline{\varepsilon}}{\partial x_j})}{\partial x_j} - C_{\varepsilon 1}\left(\overline{u_i u_j} * \frac{\partial U_i}{\partial x_j}\right)\frac{\overline{\varepsilon}}{\overline{e}} - C_{\varepsilon 2} * (\overline{\varepsilon^2}/\overline{e})$$

$$\overline{\varepsilon} = 2\vartheta\overline{S'_{ij}S'_{ij}}$$

$$\vartheta_T = C_\mu(\overline{e})^2/\overline{\varepsilon}$$

Where

$\overline{e}$ Represents the mean kinetic energy of the turbulent velocity fluctuations

$\overline{\varepsilon}$ Represents the viscous dissipation

ϑ_T Represents the eddy viscosity

$C_{\varepsilon 1}$, $C_{\varepsilon 2}$, σ_ε , σ_e are the model constants whose default values in Ansys Fluent are , 1.44, 1.92, 1.3, 1.0 respectively

Generally the k epsilon turbulence model is for initial testing before experimental analysis is done. It requires comparatively less computational resources as compared to other turbulence models. Overall, it is sufficiently accurate and versatile for many turbulence problems.

3. DIMENSIONLESS NUMBERS

Reynolds Number

The Reynolds number is defined as the ration of inertial forces to viscous forces [19].

$$Re = \frac{Inertial\ Forces}{Viscous\ Forces} = \rho VL/\mu$$

Where

ρ , V , , μ Represents density, velocity, characteristic length and dynamic viscosity of the fluid.

Grashof Number

The Grashof number is defined as the ratio of the buoyancy to viscous forces acting on a fluid [19].

$$Gr = \frac{g\beta(T_s - T_\infty)L^3}{\vartheta}$$

Where

g , β , T_s , T_∞ , L , ϑ Represent the acceleration due to gravity, volumetric thermal expansion coefficient, surface temperature, bulk temperature, characteristic length and kinematic viscosity of the fluid

Nusselt number

The Nusselt number is defined as the ratio of the convective heat transfer to conductive heat transfer [19].

$$Nu = \frac{hL}{k}$$

Where

h , L , k Represent the convective heat transfer, characteristic length, and thermal conductivity of the fluid.

Dimensionless Temperature

The dimensionless temperature T^* is defined as follows

$$T^* = \frac{T - T_m}{(h^2 * Q/k)}$$

Where

T , T_m Represents the physical temperature and the ambient temperature respectively

h , Q , k Represents the characteristic length, heat flux applied and the thermal conductivity respectively

4. NUMERICAL MODEL

The first part of this study consists of numerical analysis of forced convection in a 2D cavity. Consider a 2D cavity of aspect ratio 4, this value has been considered as the common aspect ratio among aircraft fuselages is between 3 to 6. The inlet and outlet vents are located at opposite walls of the cavity. The vents are 0.1 meters wide. The walls of the cavity are adiabatic. Heat flux is applied to a part of the bottom wall. The length to which heat flux applied is 0.2 meters. Different cases were simulated by varying the inlet Re from 30 to 1000 and the heat flux from 300 W/m^2 to 800 W/m^2. All the simulations are steady state in nature. The fluid considered is incompressible and Newtonian and the boussinesq approximation is considered. Three configurations are considered in this study

The first configuration involves the inlet vent to be at the bottom and the outlet vent to be at the top. The second involves the inlet and outlet at the bottom of the cavity. The last configuration involves both the vents to be on the same wall of the cavity. The schematic diagrams are given below

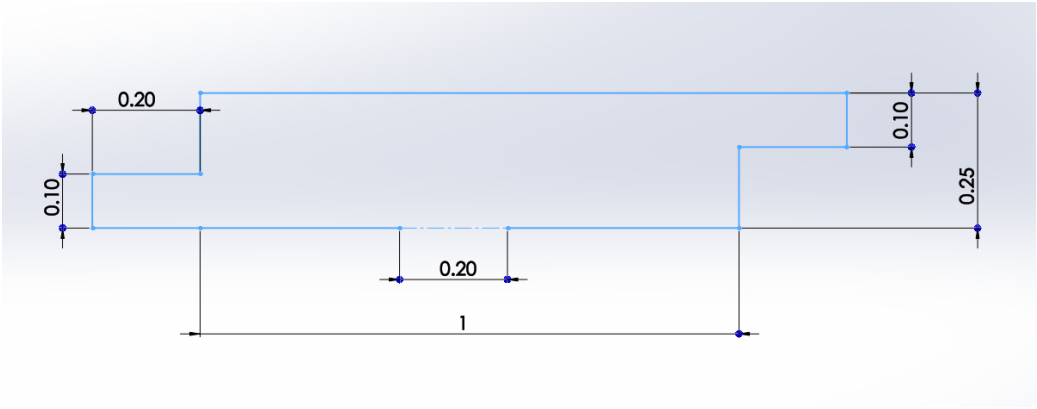

Figure 1 Laminar flow configuration 1

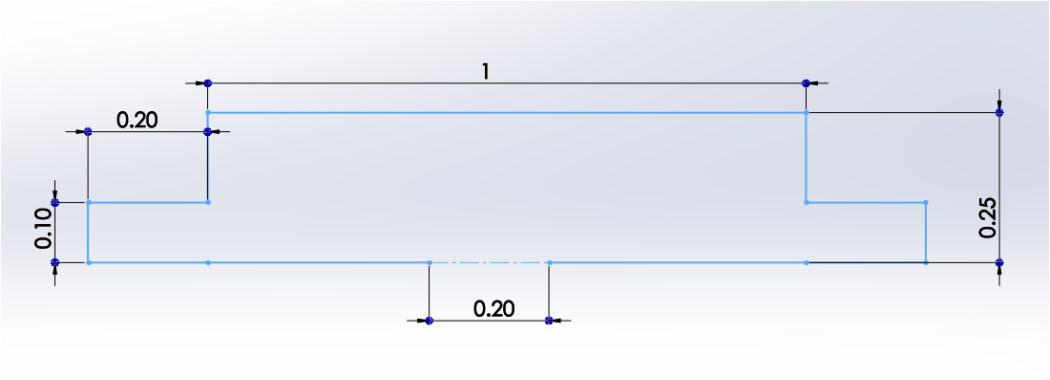

Figure 2 Laminar flow configuration 2

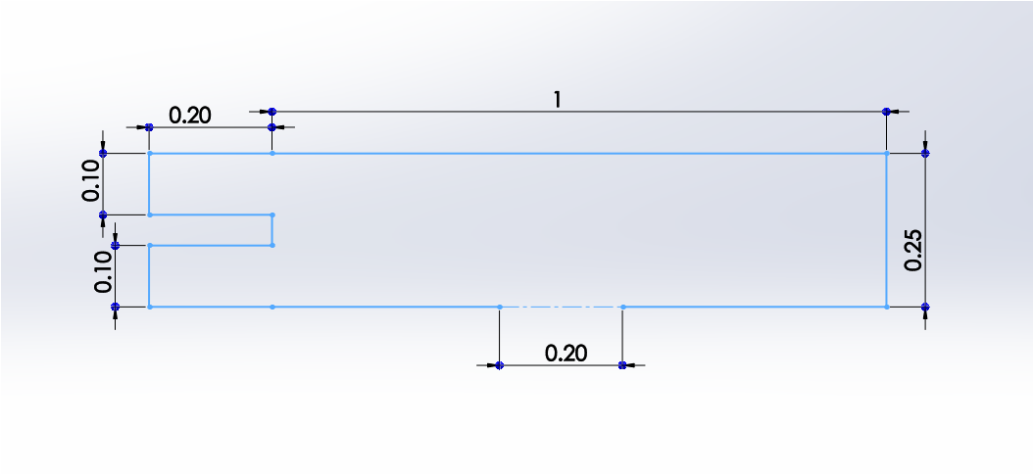

Figure 3 Laminar flow configuration 3

The second part of my thesis consists of numerical analysis of forced convection in an aircraft fuselage. The 2D cross section is modeled after the Cessna J1 business jet, which is a commercial passenger jet. The cross section of an aircraft fuselage is considered as seen from the fore of the aircraft. The radius of the fuselage is taken as 0.7 meters. Two seats are considered inside the fuselage. The seats are modelled as walls with zero thickness. Adiabatic conditions are applied to all the walls of the aircraft. The dimensions of the seats are as follows 0.4x0.2 meters. The seats are 0.4 meters apart from each other. Fire is simulated by applying heat flux to the seats. Inlets and outlet vents are situated at opposite walls of the fuselage. The inlet and outlet vents have an opening of 0.1 meters The vents simulate the ventilation or the air conditioning in an aircraft. The cases were simulated for Re 3000 and 6000. The heat fluxes applied are 1000 and

2000 W/m^2 respectively. All the simulations are transient in nature. The fluid considered is incompressible and Newtonian. The boussinesq approximation was also considered. Three configurations are considered in this study:

In the first configuration the inlet and outlet vents are situated at the bottom. The second configuration has the inlet vent at the bottom and outlet vent at the top. The third configuration has both the vents at the top.

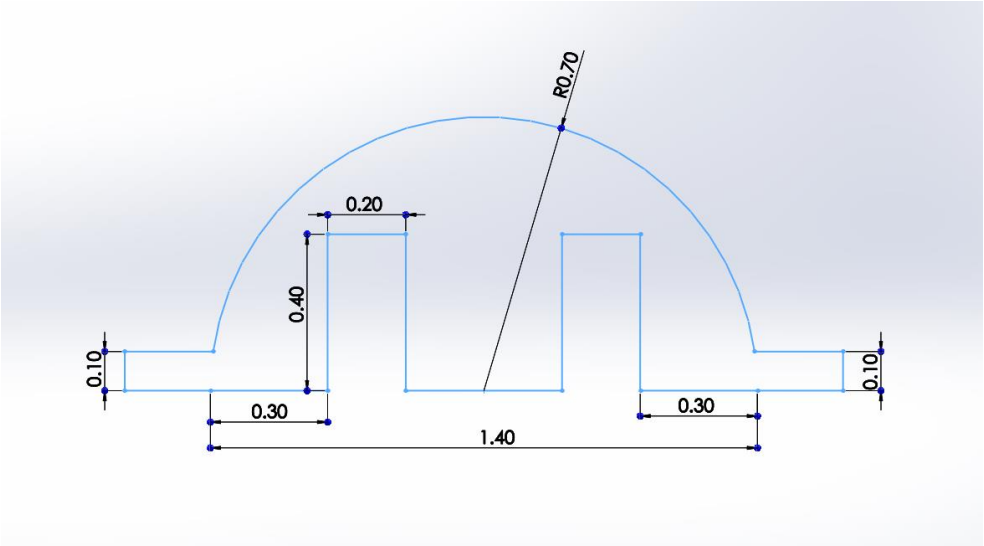

Figure 4 Turbulent flow configuration 1

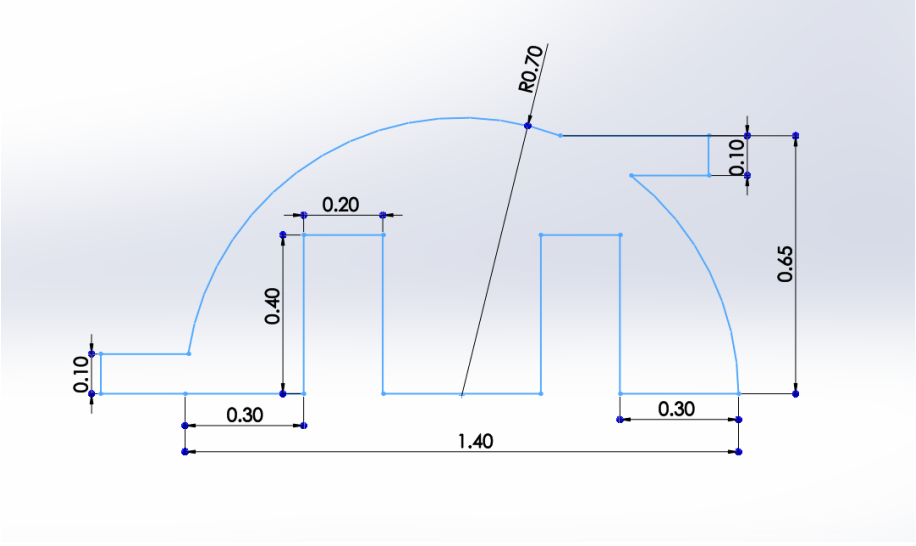

Figure 5 Turbulent flow configuration 2

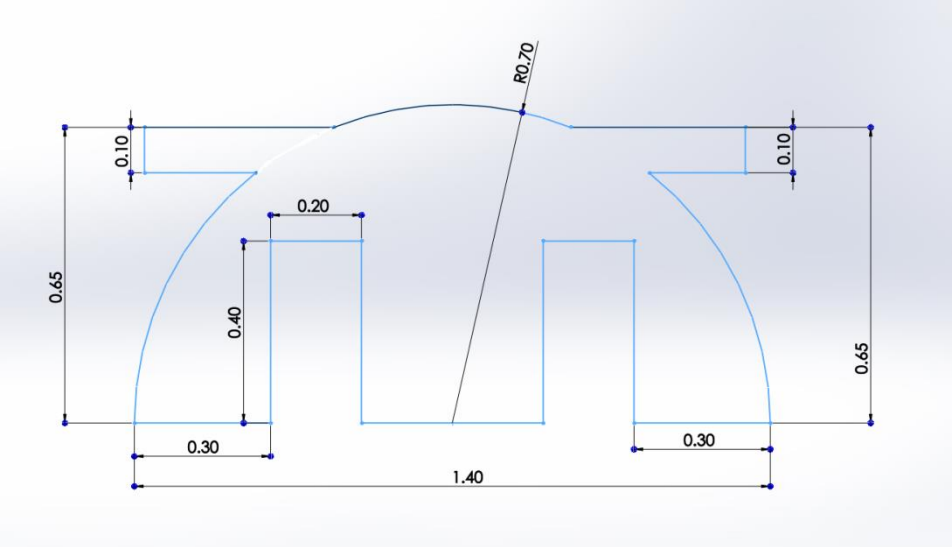

Figure 6 Turbulent flow configuration 3

5. BENCHMARK SOLUTIONS

The numerical model is benchmarked using [21]. The setup consists of a two dimensional enclosed cavity which a temperature gradient on opposite walls. Adiabatic condition is applied to the remaining two. An incompressible Navier Stokes equation with the boussinesq approximation is considered inside the enclosed cavity. The simulation is carried for Rayleigh numbers of 10^3, 10^4 and 10^5. The velocity and temperature profiles are compared with [21]. The results are in good agreement.

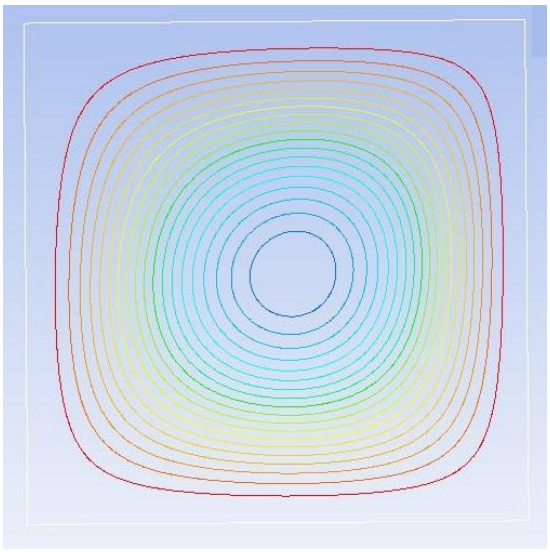

Figure 7 Streamlines at Ra of 10^3

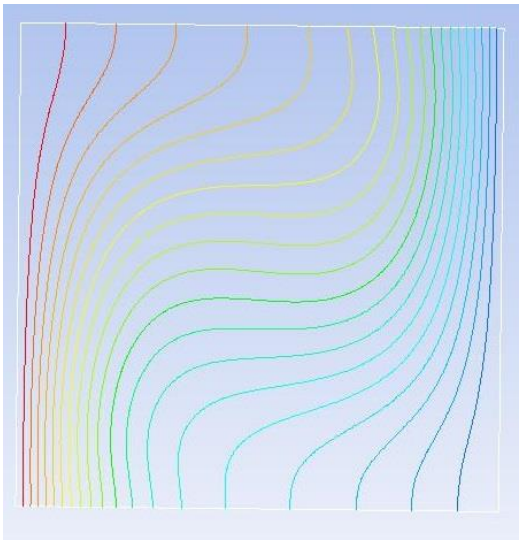

Figure 8 Temperature contours at Ra of 10^4

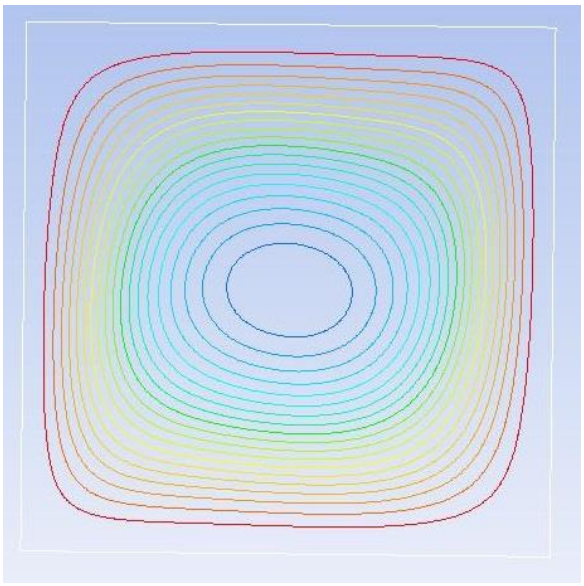

Figure 9 Streamline contours at Ra of 10^4

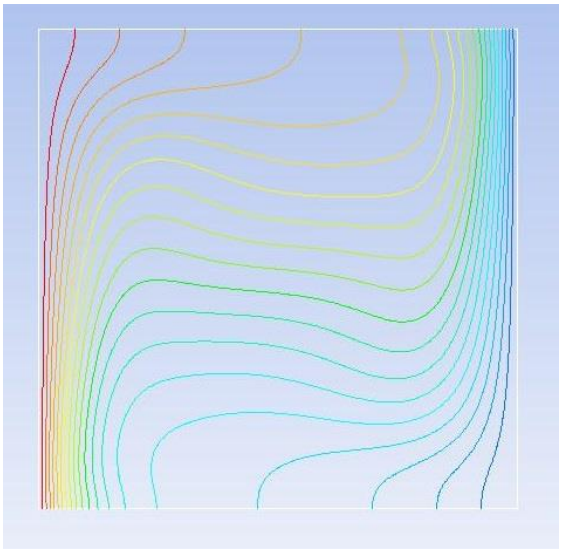

Figure 10 Temperature contours at Ra of 10^5

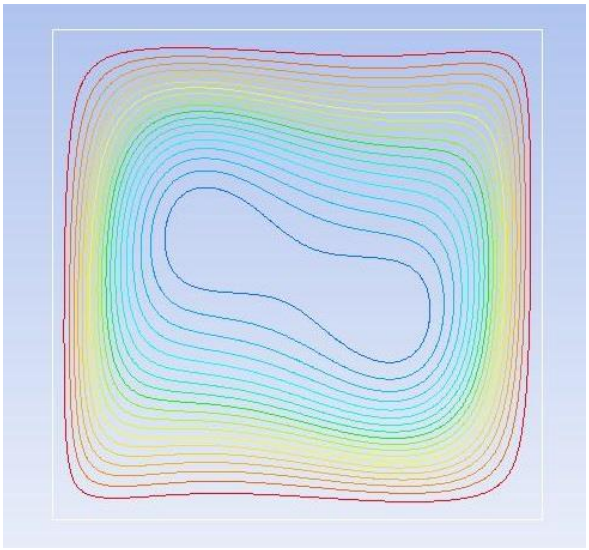

Figure 11 Streamline contours at Ra of 10^5

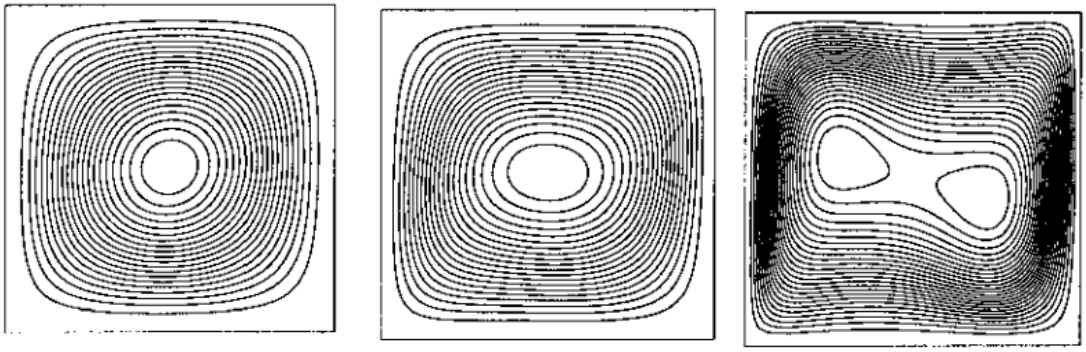

Figure 12 Benchmark Streamlines at Ra = 10^3 , 10^4 , 10^5 respectively [21]

6. GRID INDEPENDENCE

Grid independence has been shown by initially taking 360000 and then 450000 numbers of elements for configuration 1 (laminar) for Re of 1000 and heat flux of 800 W/m2. The area weighted average velocity and the temperature values at the outlet and centerline of the cavity have been taken to ensure grid independence. The values are given below.

Number of elements	Average velocity at outlet	Average velocity at centerline	Average temperature at outlet	Average temperature at centerline
36000	0.0735	0.033	320.485	313.472
45000	0.0738	0.033	320.485	313.472

7. RESULTS

A detailed analysis of the heat flow in a cavity is performed. The flow velocities and temperature profiles at the outlet and centerline are plotted. A comparative study is performed for different cavity configurations. The results are as follows.

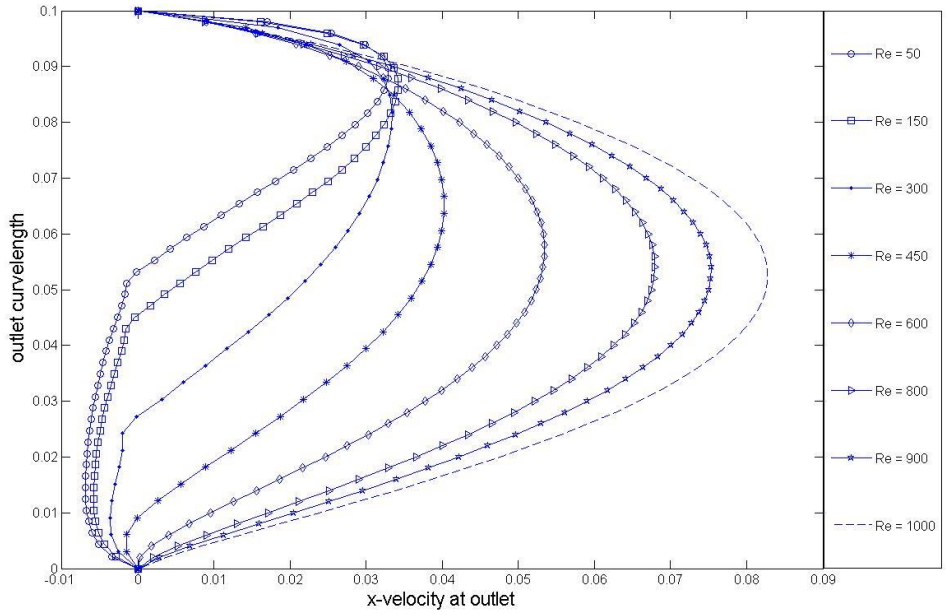

Figure 13 Plot of x component of velocity vs outlet curve length for configuration at various Reynolds number and heat flux of 500 W/m^2

The above figure is a plot of the x component of velocity at the outlet vs the outlet curve length for configuration 1. The data is plotted for increasing Reynolds number when a heat flux of 500 W/m^2 is applied to the bottom wall. Initially for lower Re number there is flow reversal at the bottom. This is due to buoyancy where the hot air exiting from the outlet rises above towards the

top and this leads to a pressure difference at the outlet. The outside air enters from the bottom. As the Re increases less amount of air enters the cavity form the surroundings until flow reversal isn't present anymore.

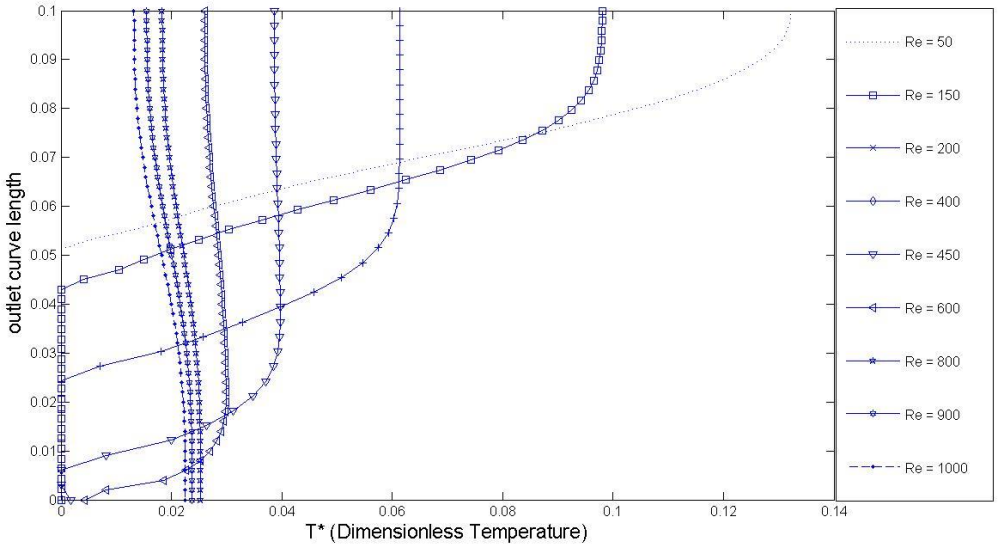

Figure 14 Plot of T* vs outlet curve length of configuration 1 for heat flux of 500 W/m^2

The above plot is of the Dimensionless temperature T* vs the outlet curve length for increasing Reynolds numbers. A heat flux of 500 W/m^2 is applied to the bottom wall. Initially low Reynolds numbers flow reversal occurs at the outlet and hence the ambient air enters the outlet at 300 K. This can be seen in the plot where initially T* is zero and increases steadily at the top of the outlet. The high temperature exits from the top of the outlet as can be seen from the plot. As the Re number increases the flow exits the outlet with an almost uniform temperature.

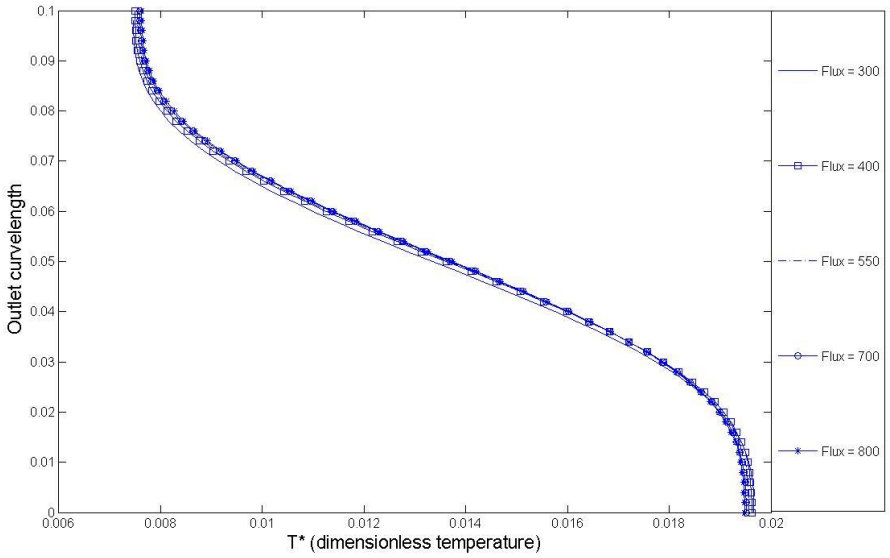

Figure 15 Plot of T*(dimensionless temperature) vs outlet curve length for laminar configuration 1 at Re=500

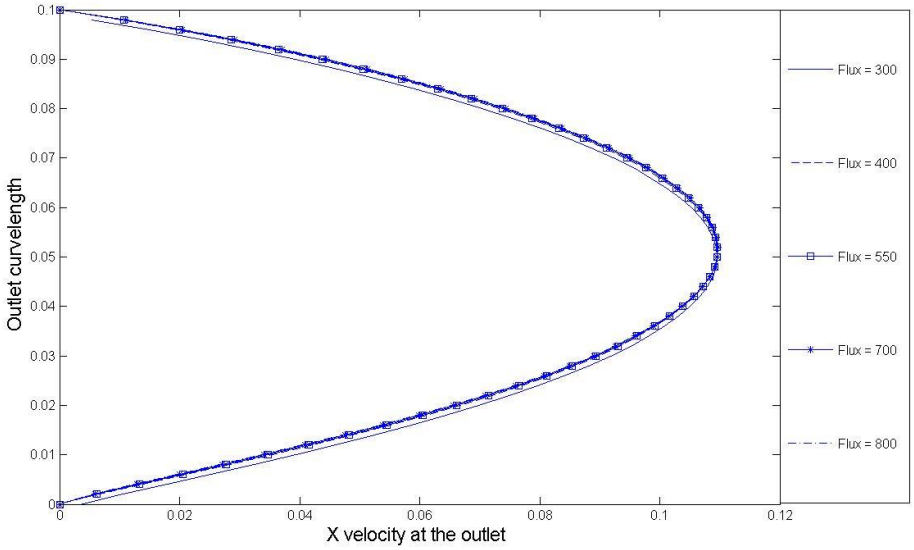

Figure 16 Plot of x component velocity vs outlet curve length for laminar configuration 1 at Re=500

The above plots show the x-component of outlet velocity and the dimensionless temperature wrt the curve length for the first laminar flow configuration. The trends are studied for Reynolds number of 500 and increasing heat fluxes from 300 W/m^2 to 800 W/m^2.The plots indicate a very similar pattern. Although the heat flux applied is increased the outlet temperatures remain almost similar, which indicates that the temperature of the cavity is increasing steadily.

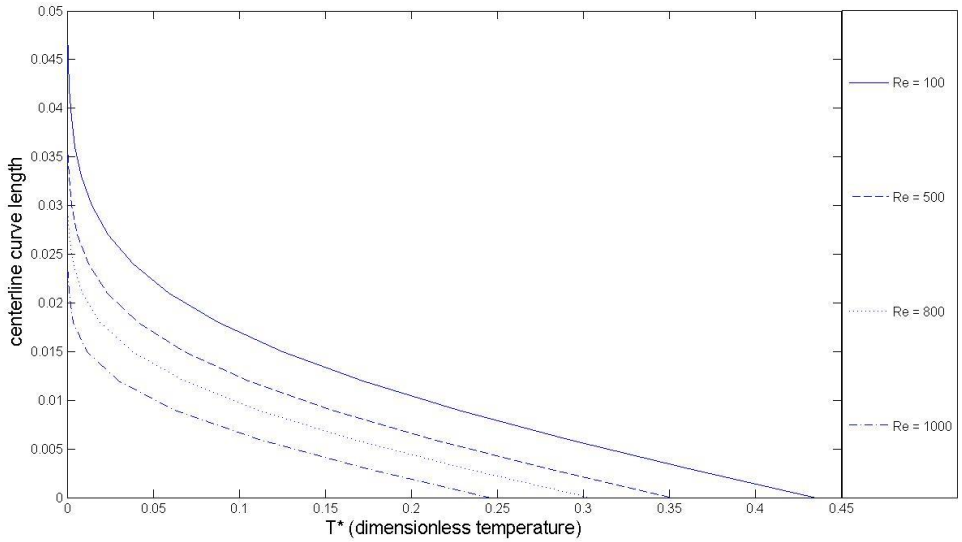

Figure 17 Plot of T* vs centerline curve length for configuration 1 for a heat flux of 500 W/m^2

The above is a plot of the dimensionless T* vs the centerline curve length for increasing Re numbers. As can be seen the temperature increases from the top to the bottom. The temperature is maximum at the bottom where the heat flux is applied and is almost 300 K at the top. The temperature decreases at the bottom for increasing Re which is obvious as more amount of heat is removed.

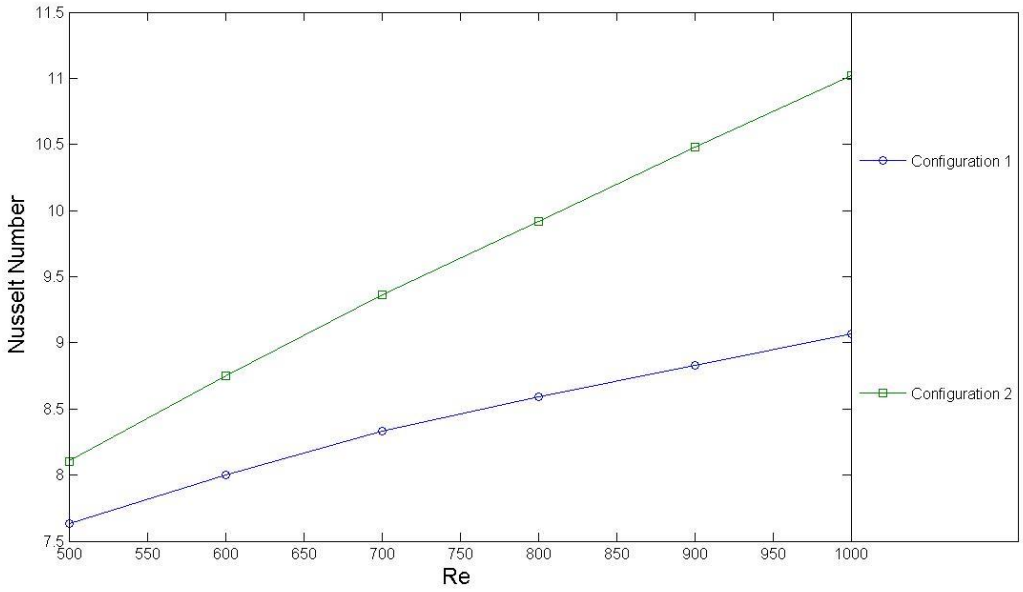

Figure 18 Comparison of Nusselt numbers of configuration 1 and 2 for varying Re

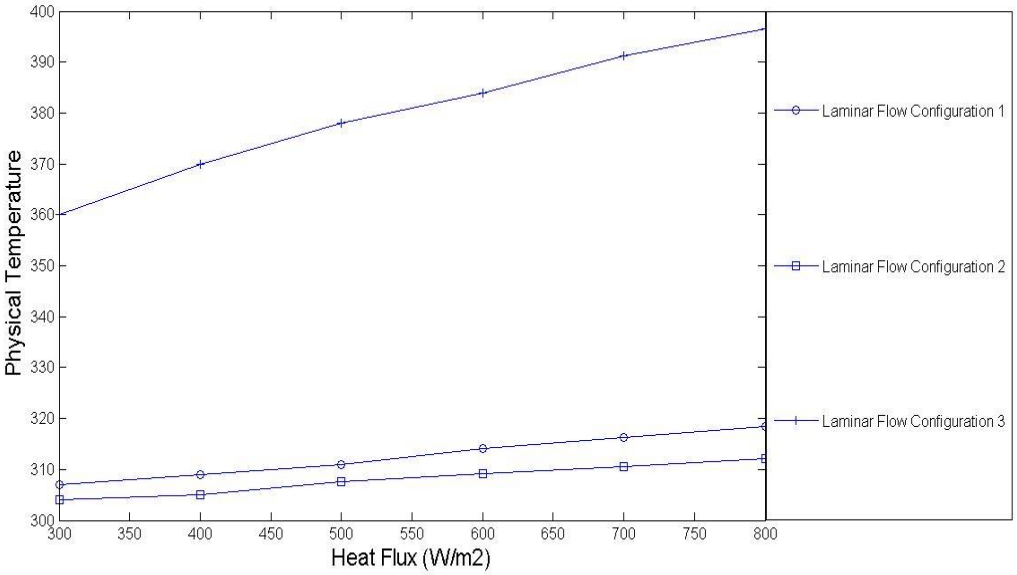

Figure 19 Plot of the physical temperature vs heat flux for all the laminar flow configurations

The above plot is of the Nusselt number vs Reynolds number for the two configurations. It is seen that the Nusselt number increases as the Reynolds number increases, this shows that convection dominates over conduction as Re increases. The values are lower for configuration 1 as compared to configuration 2 because of the outlet. The location of the outlet in configuration 2 allows for the easy exit of heat from the cavity.

The results for the turbulent flow configurations are as follows

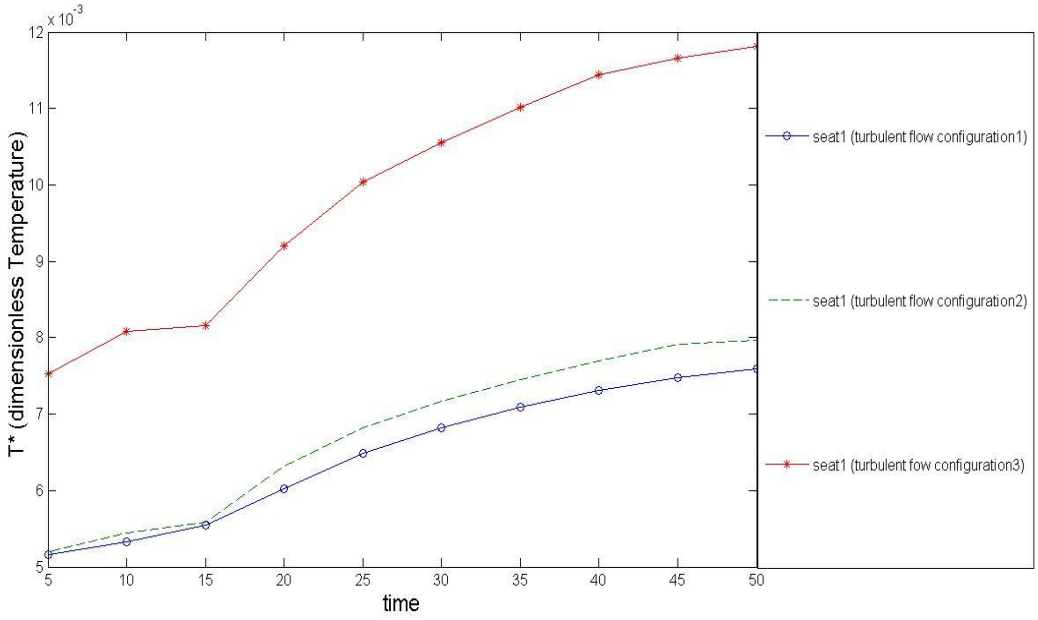

Figure 20 Plot of T* of seat 1 vs time for different configurations for Re=3000 and flux=1000 W/m^2

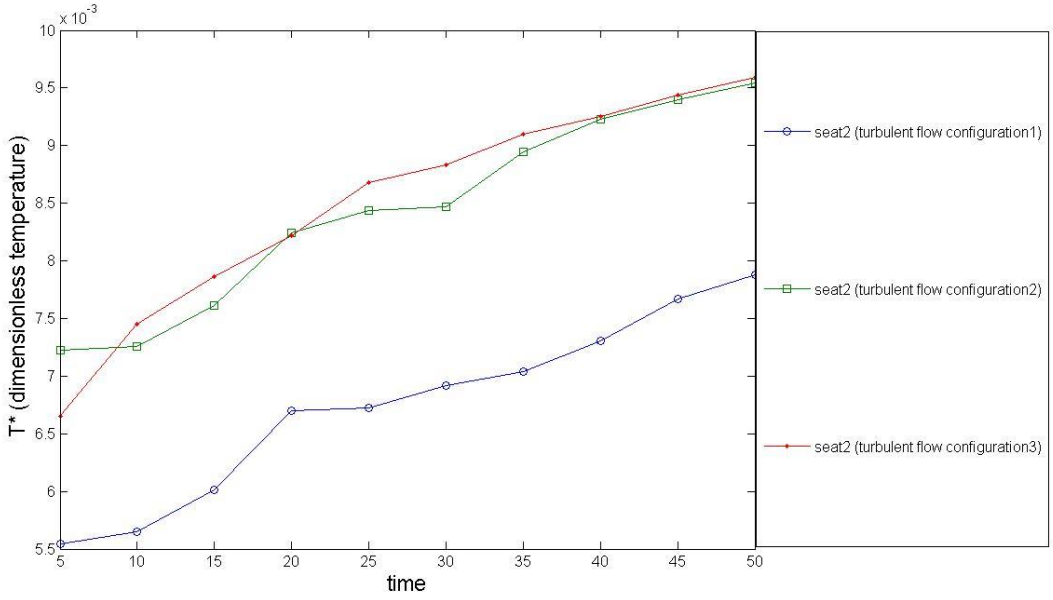

Figure 21 Plot of T* of seat 2 vs time for different configurations for Re=3000 and flux=1000 W/m^2

The above plots show the relationship between T* (dimensionless temperature) and time for seat 1 and seat 2 in different configurations. From our results it is seen that in the temperatures are least in configuration 1. The temperature difference is similar for both configurations 2 and 3. This makes case 1 the most efficient for heat removal in the time span of 50 seconds.

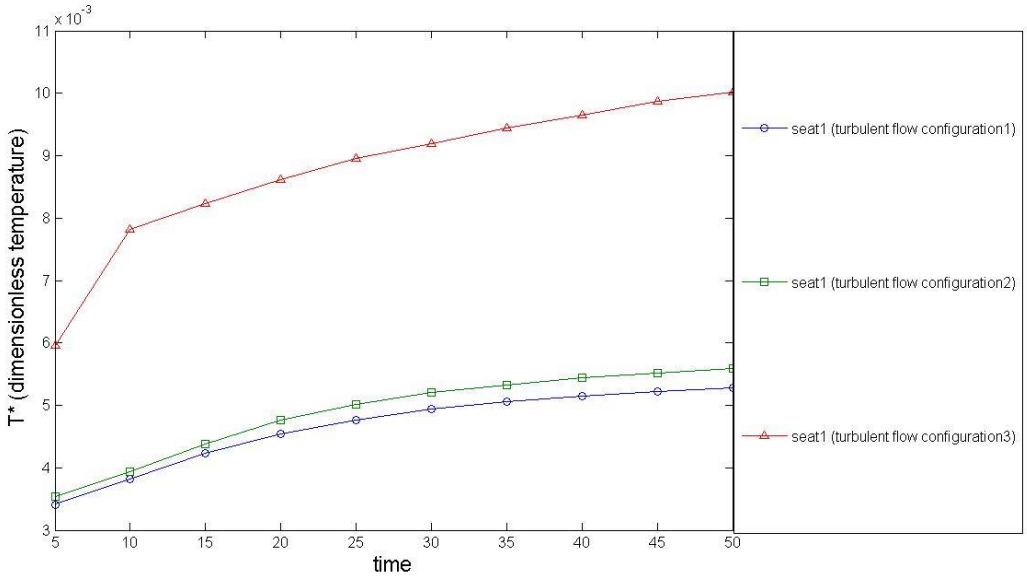

Figure 22 Plot of T* of seat 1 vs time for different configurations for Re=6000 and flux=1000 W/m^2

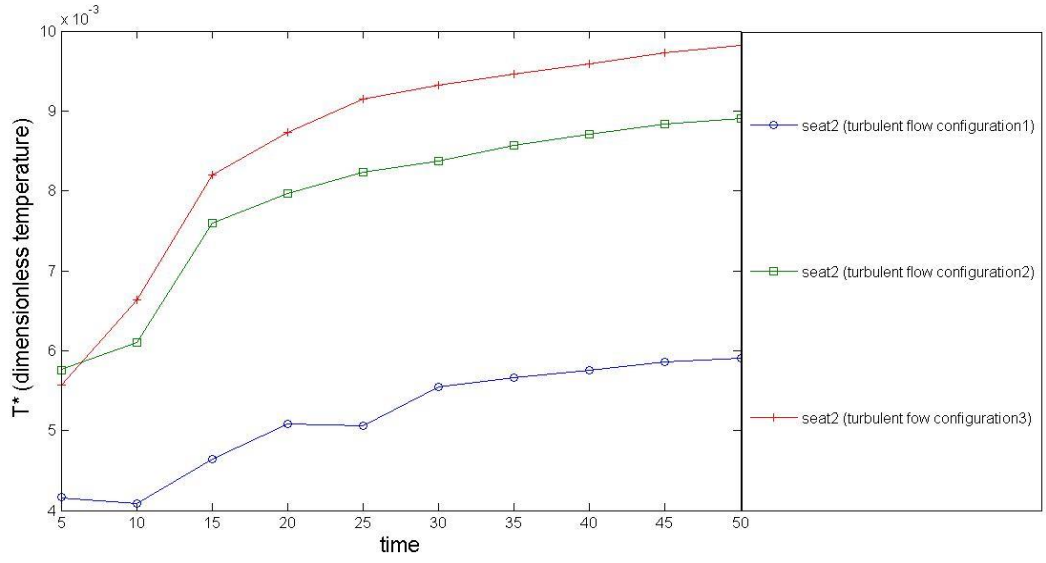

Figure 22 Plot of T* of seat 2 vs time for different configurations for Re=6000 and flux=1000 W/m^2

The above plots are of the T* (dimensionless temperature) and time. From our results we obtained that as the Re increases from 3000 to 6000, the temperatures inside the cavity decreases. Configuration 1 has the least temperatures compared to the other two.

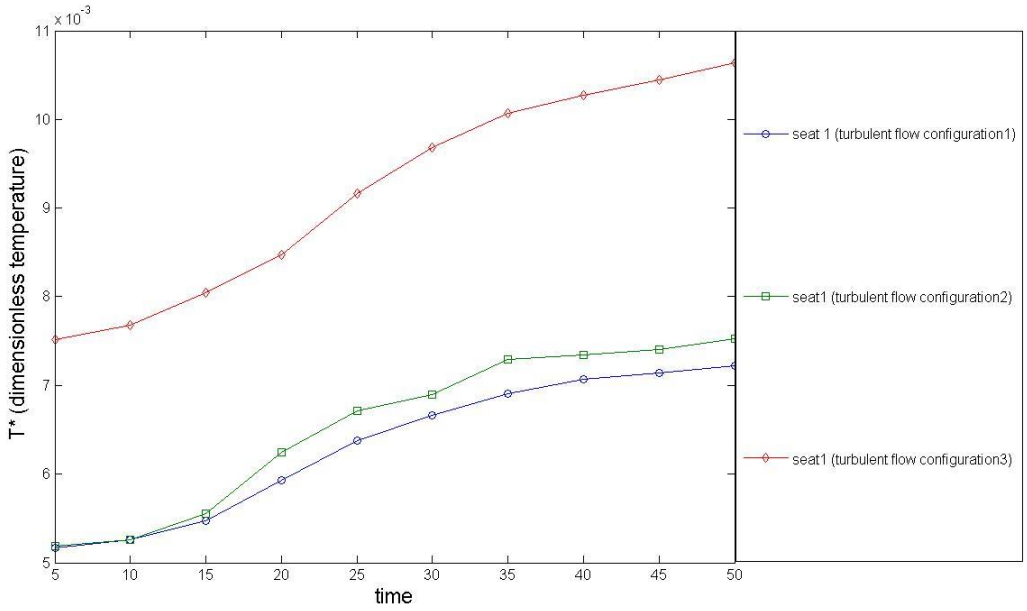

Figure 23 Plot of T* of seat 1 vs time for different configurations for Re=3000 and flux=2000 W/m^2

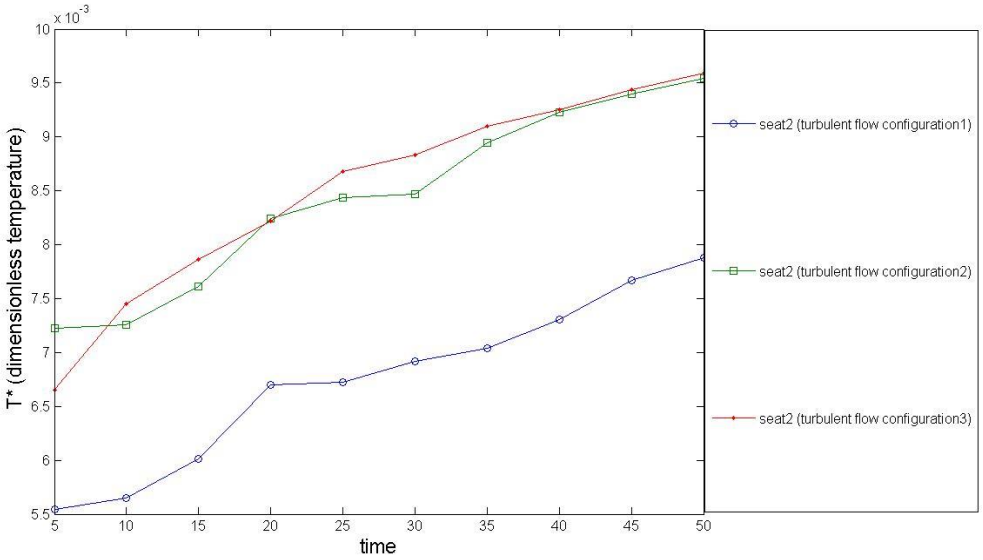

Figure 24 Plot of T* of seat 2 vs time for different configurations for Re=3000 and flux=2000 W/m^2

As the heat flux increase from 1000 W/m^2 to 2000 W/m^2 for a given Re, a similar trend is obtained. Here case 1 and case 2 have almost same seat 1 temperatures. Whereas for seat 2, case 1 still has the least temperatures out the three cases studied.

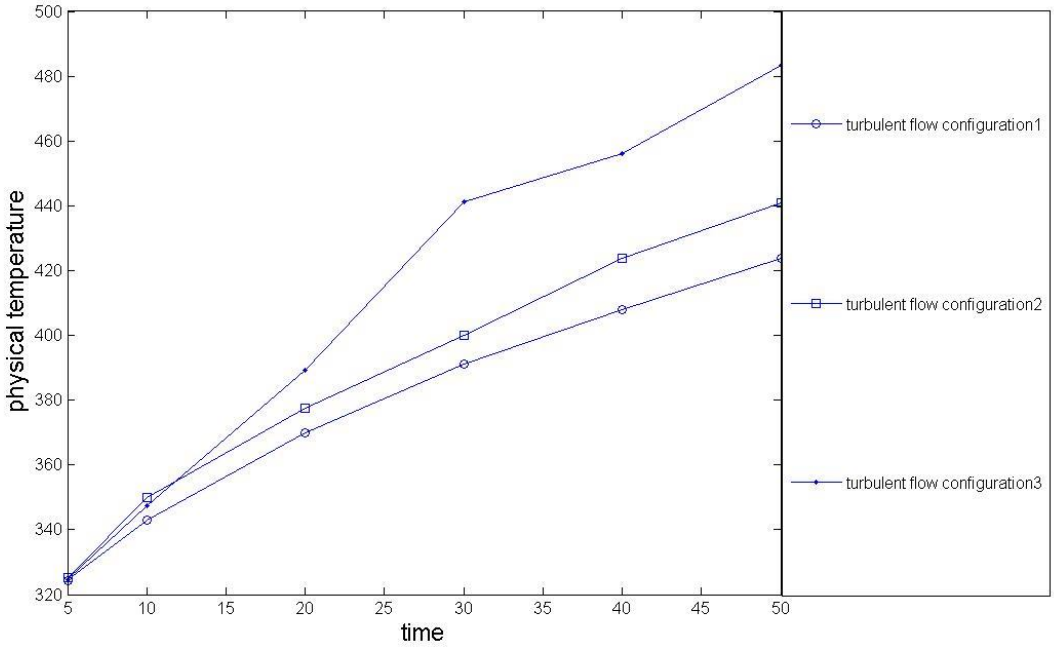

Figure 25 Plot of average temperature vs time for three turbulent flow configurations for Re=6000 and flux=1000 W/m^2

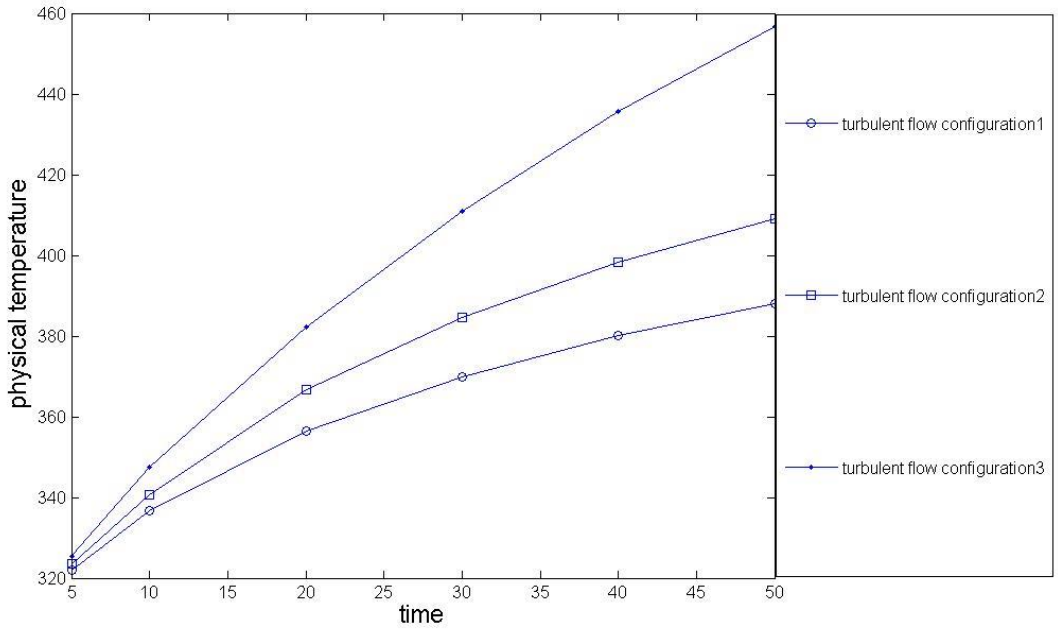

Figure 26 Plot of average temperature vs time for three turbulent flow configurations for Re=6000 and flux=2000 W/m^2

The above plots show the relative efficiency of the first turbulent configuration wrt the other two. As seen from above for a given Reynolds numbers of 3000 and 6000 and heat flux of 2000 W/m^2 respectively, the average physical temperature of the first configuration is the least. Another trend which can be seen is that at the start they all start from similar temperatures an increase linearly with time upto 50 seconds.

7.1 VELOCITY VECTOR FIELDS AND TEMPERATURE CONTOURS

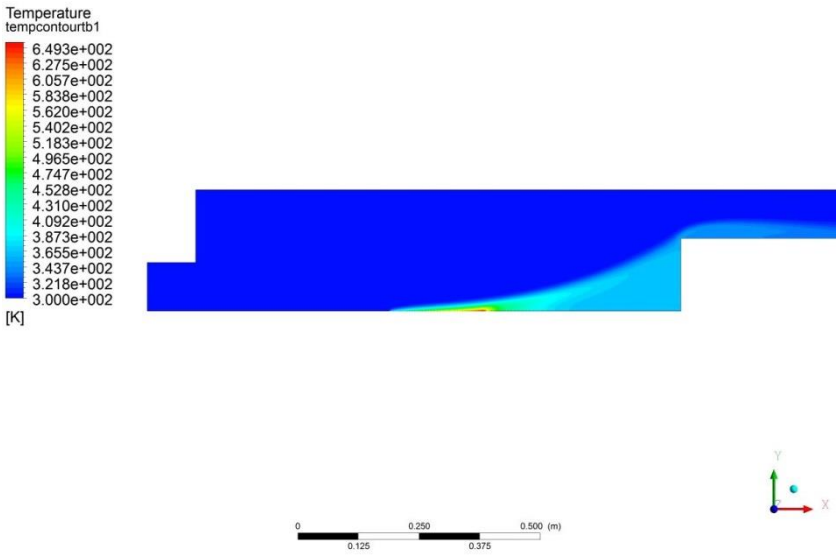

Figure 27 Temperature contour of configuration 1 (laminar case)

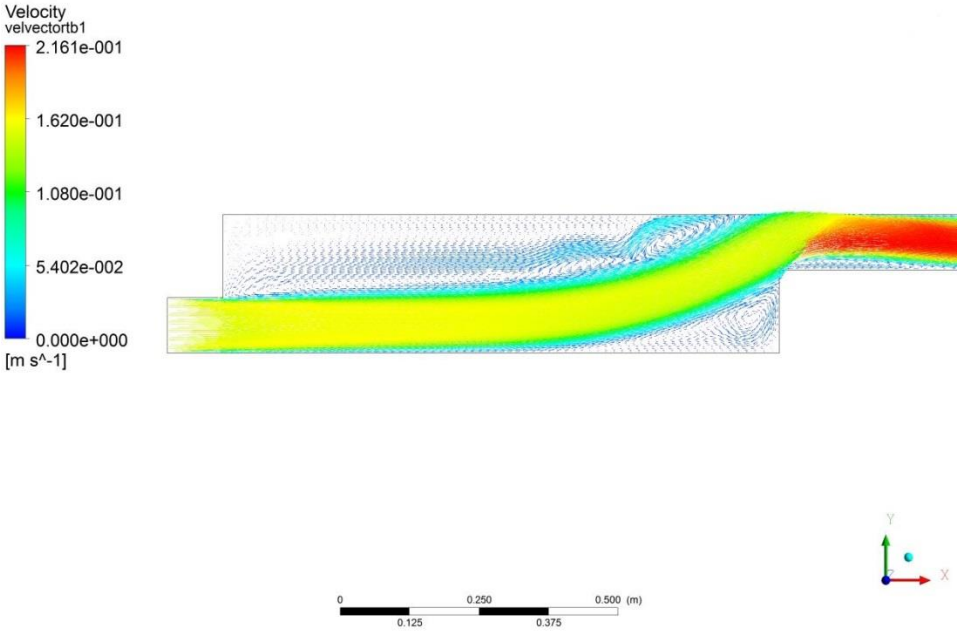

Figure 28 Velocity vectors of configuration 1 (laminar case)

The above shows the velocity vector and temperature contour of configuration 1 at Re = 1000. A heat flux of 500 W/m^2 is applied at the bottom. There is a primary vortex and many secondary vortices near the outlet where the cavity narrows. Also a vortex appears at the step near the outlet. The heat spreads to about roughly one third of the cavity, towards the right of the applied heat

flux. Most of the room remains at 300 K. Most of the heat is concentrated at the bottom right corner of the cavity. This is obvious as the inlet velocity pushes the heat generated towards the right.

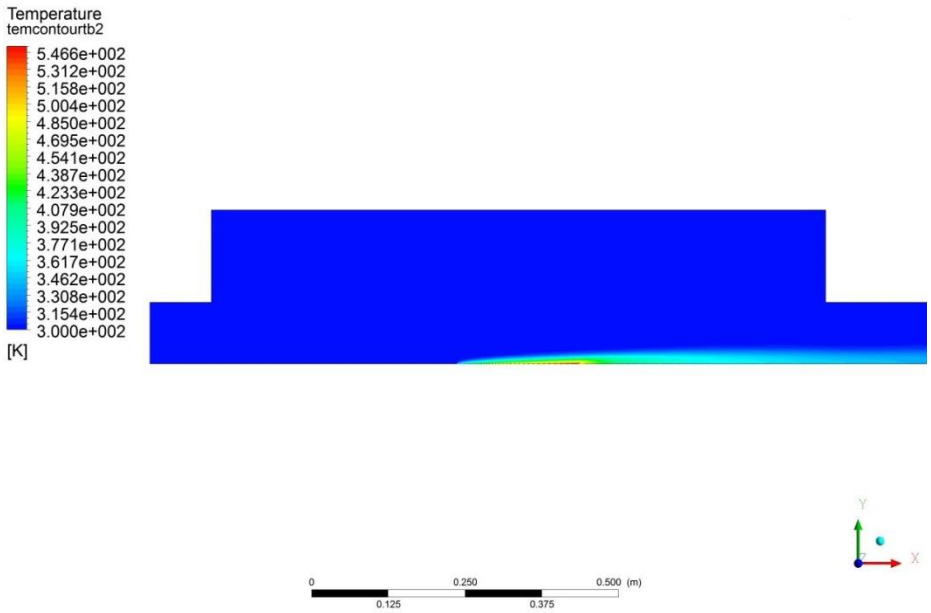

Figure 29 Temperature contour of configuration 2 (laminar case)

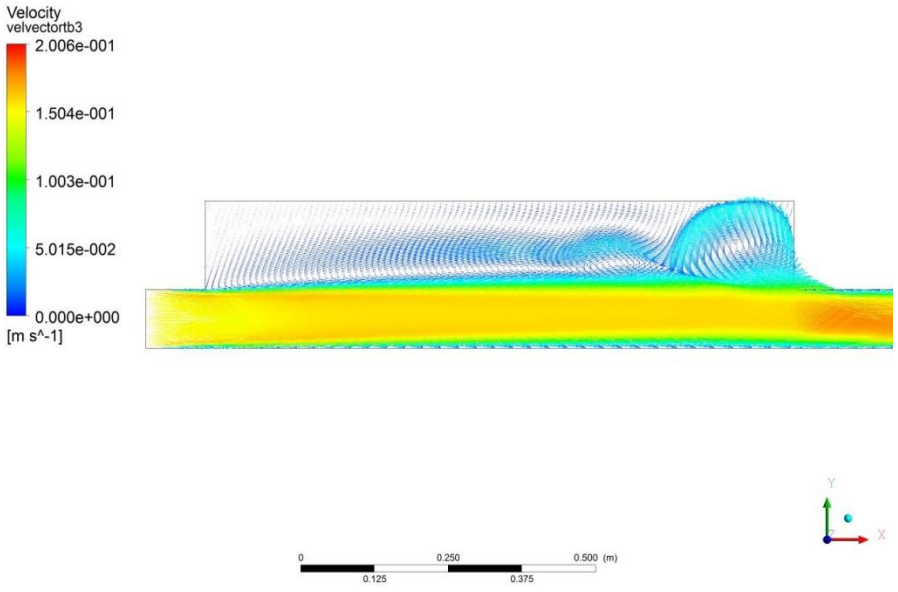

Figure 30 Velocity vectors of configuration 2 (laminar case)

The above shows the velocity vector and temperature contour of configuration 2 at Re=1000. A heat flux of 500 W/m^2 is applied at the bottom. This seems to be the most efficient way for heat removal out of the three configurations studied. The heat is carried directly to the outlet and most the cavity is at 300 K. Upon observation of the velocity vector plot we can see that there is a primary vortex near the outlet where the cavity narrows down.

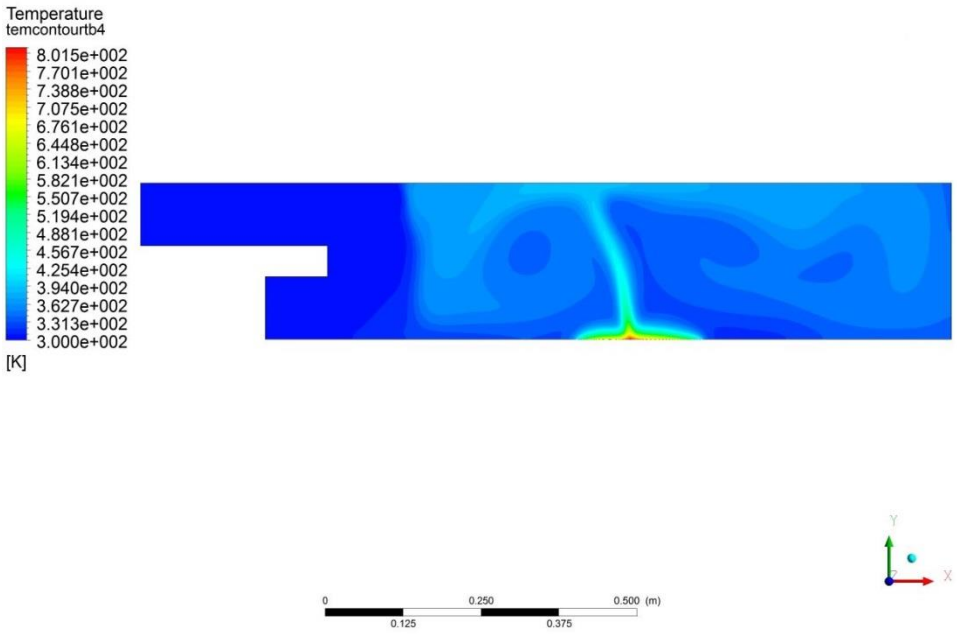

Figure 31 Temperature contour of configuration 3 (laminar case)

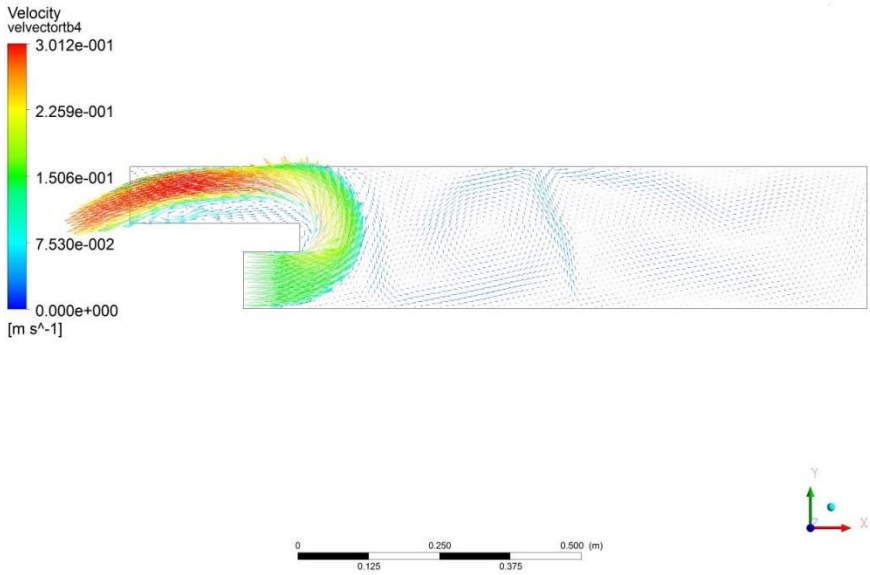

Figure 32 Velocity vectors of configuration 3 (laminar case)

The above is the temperature contour of the third configuration. As can be seen from the temperature plot most of the heat flux generated in the cavity stay in the cavity. The inlet velocity exits directly to the outlet carrying very less amount of heat with it. The average temperature of the cavity is about 600 K. This is the least efficient configuration of the three models studied.

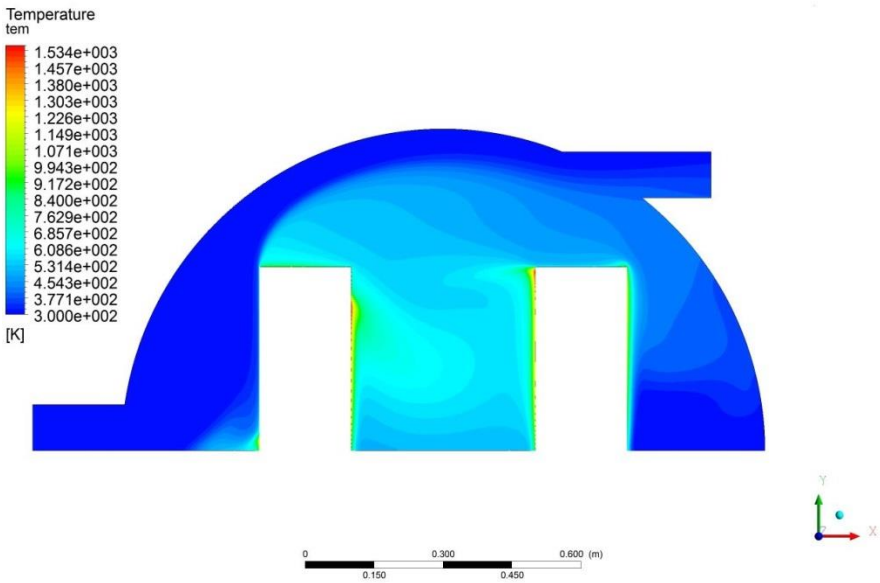

Figure 33 Temperature contours at Re=3000 and heat flux of 1000 W/m^2 at 50 seconds

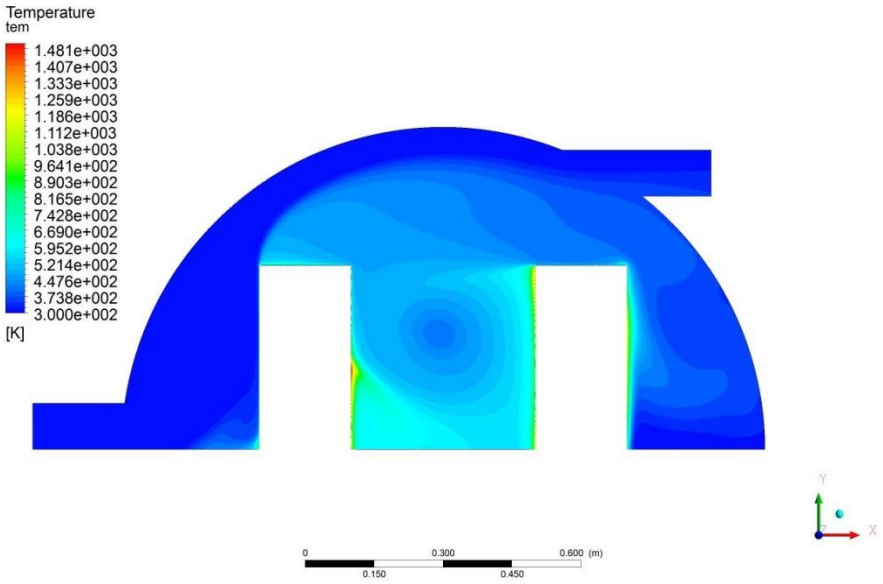

Figure 34 Temperature contours at Re=6000 and heat flux of 1000 W/m^2 at 50 seconds

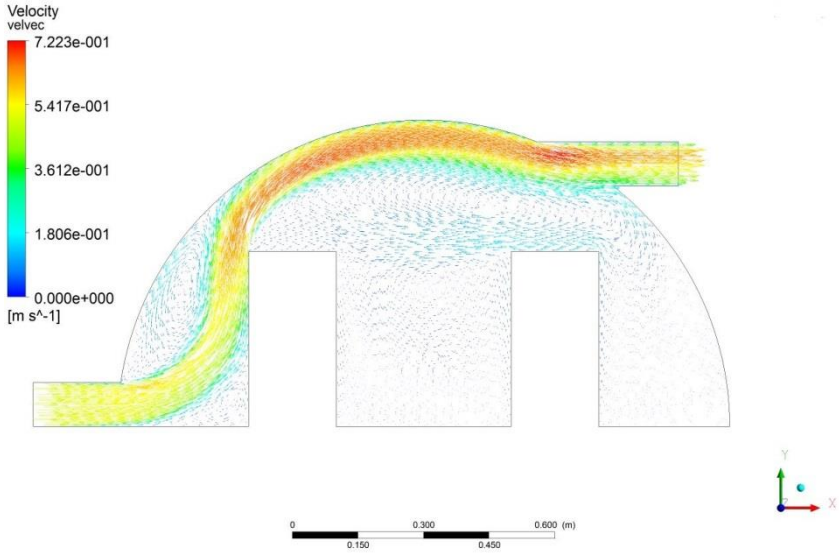

Figure 35 Velocity vector at Re=3000 and heat flux of 1000 W/m^2 at 50 seconds

The above are the temperature contours are for configuration 1. The Reynolds numbers are 3000 and 6000 respectively. From our results we see that a vortex develops between the 2 seats where most of the heat is trapped.

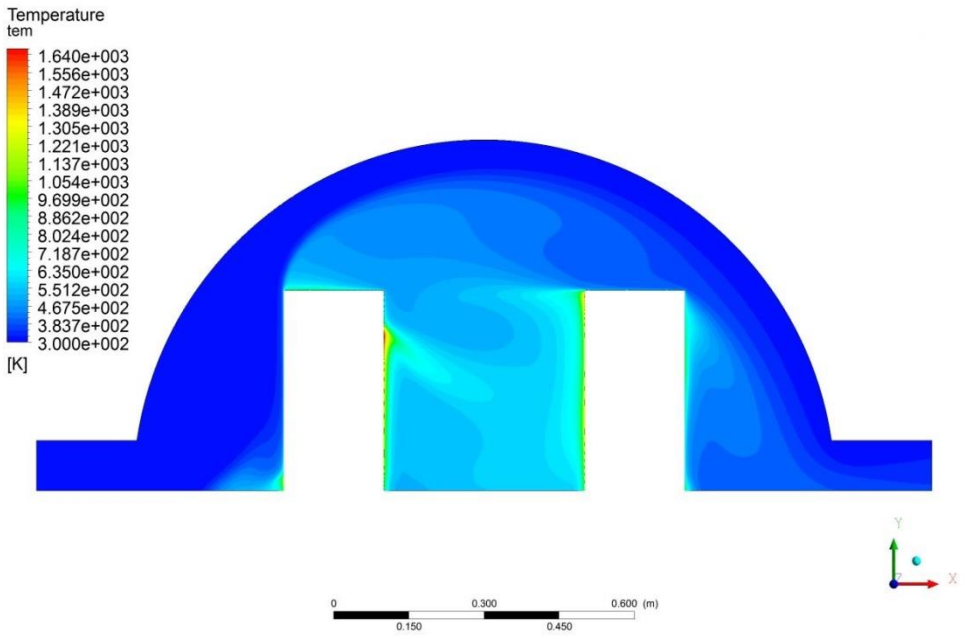

Figure 36 Temperature contours at Re=3000 and heat flux of 2000 W/m^2 at 50 seconds

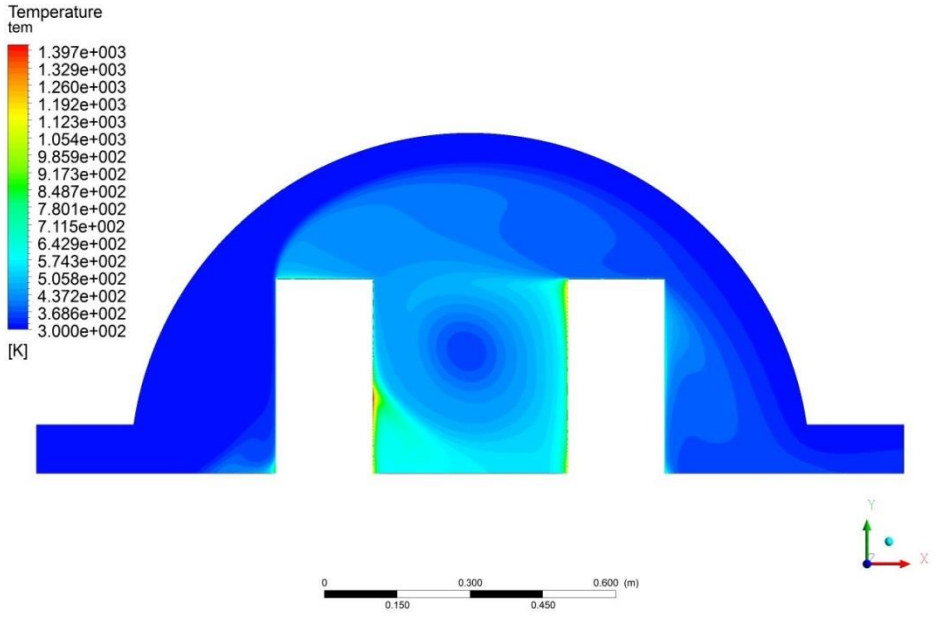

Figure 37 Temperature contours at Re=6000 and heat flux of 2000 W/m^2 at 50 seconds

The above contours show the variation of temperature in the cavity. As can be seen before a vortex develops between the two seats in the cavity.

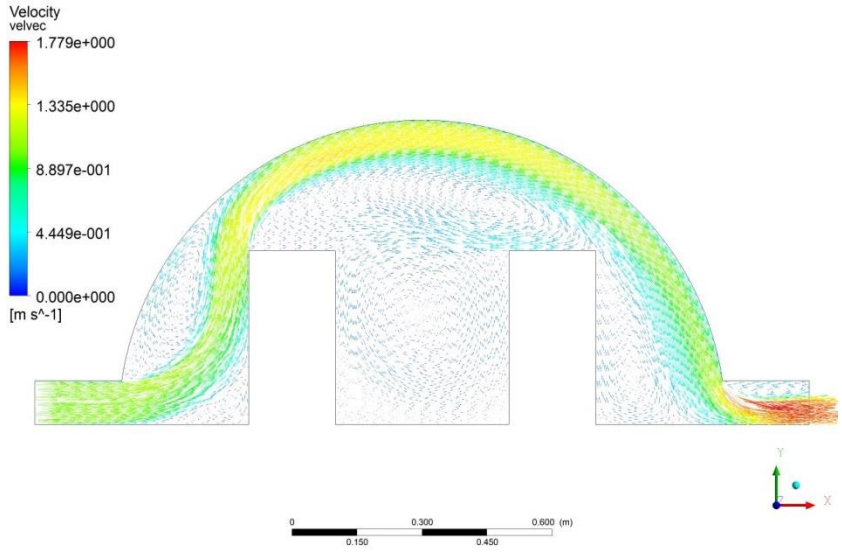

Figure 38 Velocity vector at Re=6000 and heat flux of 2000 W/m^2 at 50 seconds

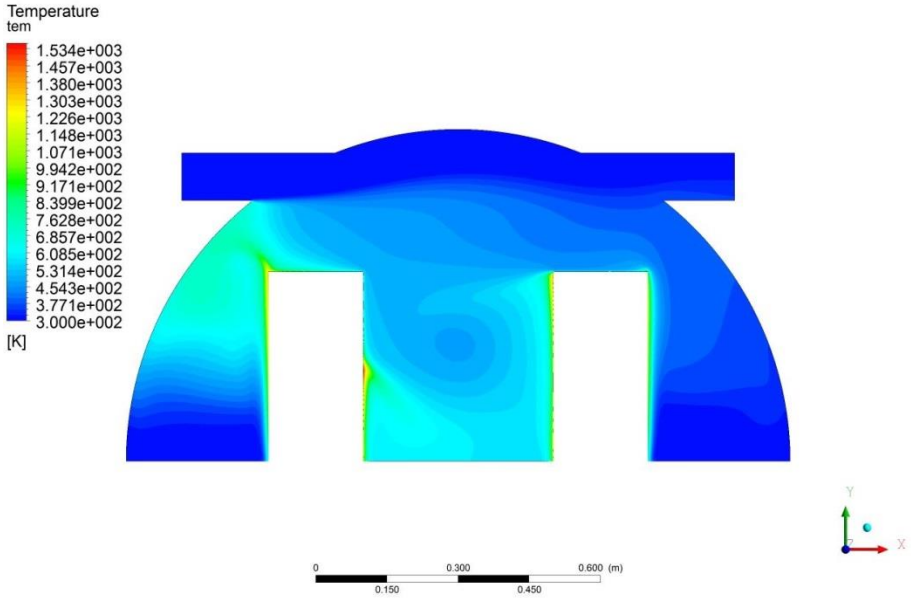

Figure 39 Temperature contours at Re=6000 and heat flux of 2000 W/m^2 at 50 seconds

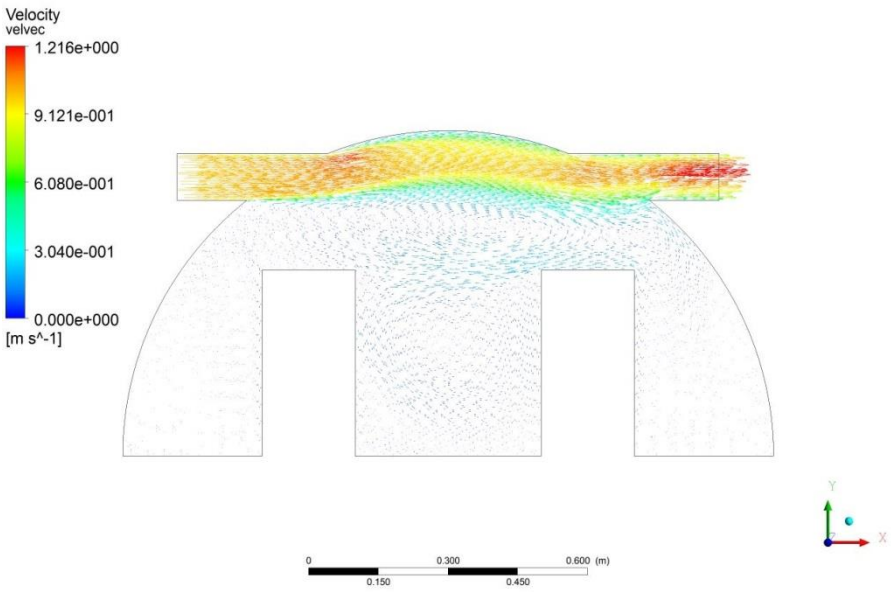

Figure 40 Velocity vector at Re=6000 and heat flux of 2000 W/m^2 at 50 seconds

The above are the temperature contours at Re=6000 and heat flux of 2000 W/m^2. From our results we concluded that the above is the least efficient of the three cases studied. Most of the heat is trapped between the two seats and in the gap between the first seat and the fuselage.

8. CONCLUSIONS

Detailed numerical analyses of the heat in a 2D cavity with buoyancy have been done in the laminar range. Three configurations have been considered. The first configuration has been simulated for Re ranging from 30 to 1000 and the heat flux from 300 W/m^2 to 800 W/m^2. The outlet velocities and temperature profiles have been studied in detail. It is been noticed that after Reynolds number of about 400 the outlet temperature profiles remain more or less the same. As the Reynolds number increases two vortices are formed at the mouth of the outlet. This inhibits the exit of heat and hence reduces the heat reduction efficiency of the configuration. A detailed analysis has been done for the second laminar flow configuration. Here due to the location of the

outlet, this is found to be the most efficient configuration. No vortices are formed in this configuration. Almost most of the cavity is at ambient temperature. The third configuration considered here has the least efficient in terms of heat reduction. Very little heat exits from the outlet and the average temperature of the cavity is about 380 K. From our results we conclude that this configuration must not be employed to rooms where constant heat removal is required. The second configuration is efficient and can be applied for heat removal purposes.

The second part of the thesis contains detailed analyses of a turbulent flow two dimensional cavity. The vents of the cavity are modeled as the air conditioning in an aircraft. K epsilon model was used for the transient turbulence cases. The Re and heat fluxes considered are 3000, 6000, 1000 W/m^2 and 2000 W/m^2 respectively. Here three configurations have been considered by changing the locations of the inlet and outlet vents and a comparative study has been conducted. In all the three configurations as the Reynolds number increases a vortex formation is noticed between the seats. This prevents the heat from exiting and increases recirculation of the hot air. Hence most of the heat is trapped in between the seats. When the seat temperatures of the three configurations are compared, we see that the first and second have similar temperatures. A transient comparative study of the average temperature of the cavities shows that the first and the second turbulent flow configurations have similar average temperatures initially but the trend diverges as time increases. The average temperature of the third configuration is much more than the other two. To further increase the efficiency with regard to heat removal we can install more vents. The vortex created can also be destroyed by perturbations in the flow field and study if they affect the heat removal efficiency. The inlet air temperature can be decreased and the effects of such a scenario can be studied. More sophisticated turbulence models can also be used which include the effects of smoke and disturbances like passenger movement in the cabin.

9. REFERENCES

[1] Md. Mamun Molla, M. M. A. Sarker, 2006, "Natural Convection Flow In A Square Cavity With Temperature Dependent Heat Generation", Proceedings of 3rd BSME-ASME International Conference on Thermal Engineering.

[2] J. Patterson, J. Imberger, 1980, "Unsteady natural convection in a rectangular cavity", Journal of Fluid Mechanics, Vol:100, part:1, pp: 65-86.

[3] N. Agrawal, S.M. Ali, K. Velusamy, S.K. Das, 2010, "Numerical Study of Natural Convection in an Enclosure with and without Boussinesq Assumption-A Comparative Study", Proceedings of the 37th National & 4th International Conference on Fluid Mechanics and Fluid Power.

[4] G.N. Ivey, 1984, "Experiments on transient natural convection", Journal of Fluid Mechanics, vol: 144, pp: 380-401.

[5] Ajay K. Prasad, Jeffrey R. Koseff, 1996, "Combined forced and natural convection heat transfer in a deep lid-driven cavity flow", Internal Journal of Heat and Mass Transfer, Volume 17, Issue 5, Pages 460-467.

[6] K. Torrance, R. Davis, K. Eike, P. Gill, D. Gutman, A. Hsui, S. Lyons, H. Zien, 1971, "Cavity flows driven by buoyancy and shear", Journal of Fluid Mechanics, vol: 51,part: 2, pp: 221-231.

[7] K. Khanafer, K. Vafai, 2000, "Buoyancy-driven flow and heat transfer in open-ended enclosures: elimination of the extended boundaries", International Journal of Heat and Mass Transfer, Volume 43, Issue 22, Pages 4087-4100.

[8] G. de Vahl Davis, R. W. Thomas, 1969, "Natural Convection between Concentric Vertical Cylinders", Physics of Fluids, 12, II-198.

[9] P. Bontoux, C. Smutek, A. Randriamampianina, B. Roux, G.P. Extremet, A.C. Hurford, F. Rosenberger, G De Vah Davis, 1986, "Numerical solutions and experimental results for three dimensional buoyancy driven flows in tilted cylinders", Advances in Space Research, Volume 6, Issue 5, Pages 155-160.

[10] G.D. Mallinson, G De Vahl Davis, 1977, "Three-dimensional natural convection in a box: a numerical study", J. Fluid Mech, volume 83, part 1, pp 1-31.

[11] C. Teodosiu, F. Kuznik, R. Teodosiu, 2014, "CFD modeling of buoyancy driven cavities with internal heat source- Application to heat rooms", Energy and Buildings, Volume 68, PartA, Pages 403-411.

[12] C.P. Sarkos, 1996, "Application of full-scale fire tests to characterize and improve aircraft postcrash fire environment", Toxicology, Volume 115, Issues 1-3, Pages 79-87.

[13] F. Jia, M.K. Patel, E.R. Galea, 2003, "Simulating the Swissair Fight 111 in-Flight Fire Using the CFD Fire Simulation Software SMARTFIRE", Fire Safety Engineering Group, University og Greenwich.

[14] P. Kundu, Ira M. Cohen, David R. Dowling, Fluid Mechanics.

[15] Skybrary, Retrieved 2014-12-15 http://skybary.aero/index.php?Fire_in_the_Air.

[16] Skybrary, Retrieved 2014-12-15 http://www.skybrary.aero?bookshelf/books/2330.pdf.

[18] Department of Fire Protection Engineering, Retrieved 2014-12-15

http://www.enfp.umd.edu/research/fire-modeling/zone.

[19] Wikipedia , Retrieved 2014-12-15 ,"Dimensionless numbers in Fluid Mechanics".

[20] CFD Online, Retrieved 2014-12-15,
http://www.cfdonline.com/Wiki/Standard_k_epsilon_model.

[21] D. C. Wan, B. S. V. Patnaik, G. W. Wei, 2001, "A New Benchmark Quality Solution For The Buoyancy-Driven Cavity By Discrete Singular Convolution", Numerical Heat Transfer, Part B, 40: 199-228.